

# Extended-soft-core Baryon-Baryon ESC08 model

## III. $S = -2$ Hyperon-hyperon/nucleon Interactions

M.M. Nagels

*Institute of Mathematics, Astrophysics, and Particle Physics  
University of Nijmegen, The Netherlands*

Th.A. Rijken\*

*Institute of Mathematics, Astrophysics, and Particle Physics  
University of Nijmegen, The Netherlands and  
Nishina Center for Accelerator-Based Science, Institute for Physical  
and Chemical Research (RIKEN). Wako, Saitama, 351-0198, Japan*

Y. Yamamoto†

*Nishina Center for Accelerator-Based Science, Institute for Physical  
and Chemical Research (RIKEN). Wako, Saitama, 351-0198, Japan*

(Dated: version of: August 23, 2018)

This paper presents the Extended-Soft-Core (ESC) potentials ESC08c for baryon-baryon channels with total strangeness  $S = -2$ . The potential models for  $S = -2$  are based on SU(3) extensions of potential models for the  $S = 0$  and  $S = -1$  sectors, which are fitted to experimental data. Flavor SU(3)-symmetry is broken only 'kinematically' by the masses of the baryons and the mesons. For the  $S = -2$  channels no experimental scattering data exist, and also the information from hypernuclei is rather limited. Nevertheless, in the fit to the  $S = 0$  and  $S = -1$  sectors information from the NAGARA event and the  $\Xi$ -well-depth has been used as constraints to determine the free parameters in the simultaneous fit of the  $NN \oplus YN \oplus YY$  data. Therefore, the potentials for the  $S = -2$  sectors are mainly determined by the NN-, YN-data, and SU(3)-symmetry. Various properties of the potentials are illustrated by giving results for scattering lengths, bound states, phase-parameters, and total cross sections.

Notably is the prediction of a bound state  $D^*$  in the  $\Xi N(^3S_1, I = 1)$ -channel with a binding energy  $B_E = 1.56$  MeV. This state is "deuteron-like" i.e. a member of the  $\{10^*\}$ -decuplet. As for the normal deuteron  $D = pn(^3S_1 - ^3D_1)$  the strong tensor force is responsible for this state.

The features of  $\Xi$  hypernuclei predicted by ESC08c are studied on the basis of the G-matrix approach. The well-depth  $U_\Xi = -7.0$  MeV and the  $\Xi N - \Lambda\Lambda$  conversion width is  $\Gamma_\Xi^c = 4.5$  MeV.

PACS numbers: 13.75.Ev, 12.39.Pn, 21.30.-x

### I. INTRODUCTION

In this paper, the third in a series of papers following [1, 2], henceforth referred to as I and II respectively, on the results and predictions of the Extended-soft-core (ESC) model for low energy baryon-baryon interactions. It presents the next phase in the development of the ESC-models and is the follow up of the ESC04-models [3–5] and the ESC08a,b-models [6] for  $S = 0, -1, -2$ . In [7] the Nijmegen soft-core one-boson-exchange (OBE) interactions NSC97a-f for baryon-baryon (BB) systems for  $S = -2, -3, -4$  were presented.

For the  $S = -2$  YY and YN channels hardly any experimental scattering information is available, and also the information from hypernuclei is very limited. There are data on double  $\Lambda\Lambda$ -hypernuclei, which recently became very much improved by the observation of the Nagara-

event [8]. This event indicates that the  $\Lambda\Lambda$ -interaction is rather weak, in contrast to the estimates based on the older experimental observations [9, 10].

In the absense of experimental scattering information, we assume that the potentials obey (broken) flavor SU(3) symmetry. As in I and II, the potentials are parametrized in terms of meson-baryon-baryon, and meson-pair-baryon-baryon couplings and gaussian form factors as well as diffractive couplings. This enables us to include in the interaction one-boson-exchange (OBE), two-pseudoscalar-exchange (TME), and meson-pair-exchange (MPE), and diffractive contributions without any new parameters. All parameters have been fixed by a simultaneous fit to the  $NN$  and  $YN$  data, with the constraints imposed (i) for  $\Lambda\Lambda(^1S_0)$  from the NAGARA event, and (ii) for the well-depth  $U_\Xi$ . The latter is assumed to be attractive and is the main reason for the occurrence of the "deuteron-like" state in the ESC08-model. For the procedure see the description in I and II. This way, each  $NN \oplus YN$ -model leads to a  $YY$ -model in a well defined way, and the predictions for the  $\Lambda\Lambda$ - and  $\Xi N$ -channels contain no ad

---

\*t.rijken@science.ru.nl

†yamamoto@tsuru.ac.jp

hoc free parameters. We have chosen for ESC08c the options: SU(3)-symmetry for of coupling constants, and pseudovector coupling for the pseudoscalar mesons. (In ESC04 also alternative options were investigated, but it appeared that there is no reason to choose any of these.) Then, SU(3)-symmetry allows us to define all coupling constants needed to describe the multi-strange interactions in the baryon-baryon channels occurring in  $\{8\} \otimes \{8\}$ . Quantum-chromodynamics (QCD) is, as is generally accepted now, the physical basis of the strong interactions. Since in QCD the gluons are flavor blind, SU(3)-symmetry is a basic symmetry, which is broken by the chiral-symmetry-breaking at low energies. This picture supports our assumptions, stated above, on SU(3)-symmetry. As is shown in [3, 4] the coupling constants and the  $F/(F+D)$ -ratio's used in the ESC04-models follow the predictions of the  $^3P_0$ -pair creation model (QPC) [11] rather closely. The same is the case for the ESC08-models, see paper I and Ref. [12] for details. Now, it has been shown that in the strong-coupling Hamiltonian lattice formulation of QCD, the flux-tube model, that this is indeed the dominant picture in flux-tube breaking [13]. Therefore, since the ESC-models are very much in line with the Quark-model and QCD, the predictions for the  $S = -2$ -channels should be rather realistic.

The material in this paper is organized by the following considerations:

Most of the details of the SU(3) description are well known. In particular for baryon-baryon scattering the details can be found in papers I, II, and e.g. [7, 14, 15]. Here we restrict ourselves to a minimal exposition of these matters that is necessary for the readability of this paper. Therefore, in Sec. II we first review for  $S = -2$  the baryon-baryon multi-channel description, and present the SU(3)-symmetric interaction Hamiltonian describing the interaction vertices between mesons and members of the  $J^P = (1/2)^+$  baryon octet, and define their coupling constants. We then identify the various channels which occur in the  $S = -2$  baryon-baryon systems. In appendix A the potentials on the isospin basis are given in terms of the SU(3)-irreps. In most cases, the interaction is a multi-channel interaction, characterized by transition potentials and thresholds. Details were given in [7, 14]. For the details on the pair-interactions, we refer to paper I and II [1, 2]. In Sec. III we give a general treatment of the problem of flavor-exchange forces, which is very helpful to understand the proper treatment of exchange forces and the treatment of baryon-baryon channels with identical particles. In Sec. V we describe briefly the treatment of the multi-channel thresholds in the potentials. In Sec. VI we present the results of the ESC08c potentials for all the sectors with total strangeness  $S = -2$ . We give the couplings and  $F/(F+D)$ -ratio's for OBE-exchanges of ESC08c. Similarly, tables with the pair-couplings are shown in appendix B. We give the  $S$ -wave scattering

lengths, discuss the possibility of bound states in these partial waves. Also, we give the S-matrix information for the elastic channels in terms of the Bryan-Klarsfeld-Sprung (BKS) phase parameters [16–18], or in the Kabir-Kermode (KK) [19] format. Tables with the BKS-phase parameters are displayed in appendix C. Such information is very useful for example for the construction of the  $\Lambda$ -,  $\Sigma$ -, and  $\Xi$ -nucleus potentials. We also give results for the total cross sections for all leading channels.

Important differences among the different versions of the ESC-models appear in the  $\Xi N$  sectors. Table XXV in Ref. [4] demonstrates that ESC04a,b (ESC04c,d) lead to repulsive (attractive)  $\Xi$  potentials in nuclear matter. In ESC08c, and also ESC08a/b/a" [20], the  $\Xi N$  interactions is attractive enough to produce various  $\Xi$  hypernuclei. A notable advantage of ESC08 over ESC04 is the occurrence of a "deuteron-like" bound state in the  $I=1$  channel, which is accessible in a  $K^- K^+$ -transition  $\Xi$ -production experiment at JPARC. Therefore, it is very interesting to study the ESC08 interactions in the G-matrix approach to baryonic matter. In Sec. VII, we represent the  $\Xi N$  G-matrix interactions derived from ESC08c as density-dependent local potentials. Here, structure calculations for  $\Xi$  hypernuclei are performed with use of  $\Xi$ -nucleus folding potentials obtained from the G-matrix interactions. It is discussed how the features of ESC08c appear in the level structure of  $\Xi$  hypernuclei. We conclude the paper with a summary and some final remarks in Sec. VIII.

## II. CHANNELS, POTENTIALS, AND SU(3) SYMMETRY

### A. Multi-channel Formalism

In this paper we consider the baryon-baryon reactions with  $S = -2$

$$A_1(p_a, s_a) + B_1(p_b, s_b) \rightarrow A_2(p'_a, s'_a) + B_2(p'_b, s'_b) \quad (2.1)$$

Like in Ref.'s [14, 15] we will for the  $YN$ -channels also refer to  $A_1$  and  $A_2$  as particles 1 and 3, and to  $B_1$  and  $B_2$  as particles 2 and 4. For the kinematics and the definition of the amplitudes, we refer to paper I [3] of this series. Similar material can be found in [15]. Also, in paper I the derivation of the Lippmann-Schwinger equation in the context of the relativistic two-body equation is described.

On the physical particle basis, there are five charge channels:

$$\begin{aligned} q = +2 : \quad & \Sigma^+ \Sigma^+ \rightarrow \Sigma^+ \Sigma^+, \\ q = +1 : \quad & (\Xi^0 p, \Sigma^+ \Lambda, \Sigma^0 \Sigma^+) \rightarrow (\Xi^0 p, \Sigma^+ \Lambda, \Sigma^0 \Sigma^+), \\ q = 0 : \quad & (\Lambda \Lambda, \Xi^0 n, \Xi^- p, \Sigma^0 \Lambda, \Sigma^0 \Sigma^0, \Sigma^- \Sigma^+) \rightarrow \\ & (\Lambda \Lambda, \Xi^0 n, \Xi^- p, \Sigma^0 \Lambda, \Sigma^0 \Sigma^0, \Sigma^- \Sigma^+), \\ q = -1 : \quad & (\Xi^- n, \Sigma^- \Lambda, \Sigma^- \Sigma^0) \rightarrow (\Xi^- n, \Sigma^- \Lambda, \Sigma^- \Sigma^0), \\ q = -2 : \quad & \Sigma^- \Sigma^- \rightarrow \Sigma^- \Sigma^-. \end{aligned} \quad (2.2)$$

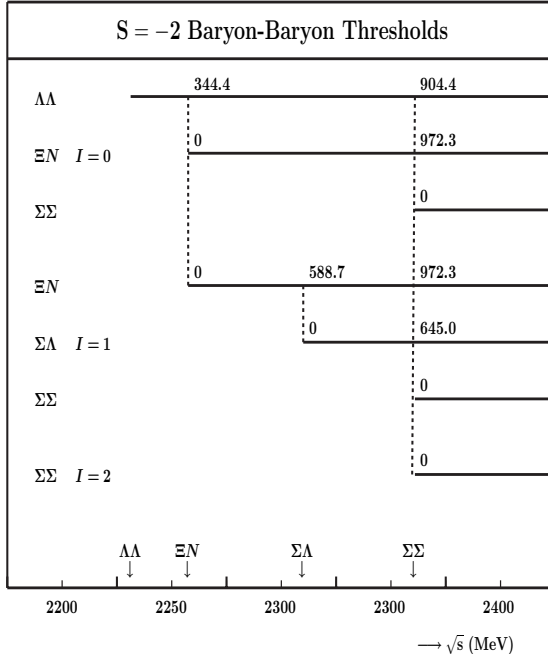


FIG. 1: Thresholds in  $YN$ - and  $YY$ -channels for  $S = -2$ .

Like in [14, 15], the potentials are calculated on the isospin basis. For  $S = -2$  hyperon-nucleon systems there are three isospin channels:

$$\begin{aligned} I = 0 : & (\Lambda\Lambda, \Xi N, \Sigma \Sigma \rightarrow \Lambda\Lambda, \Xi N, \Sigma \Sigma), \\ I = 1 : & (\Xi N, \Sigma \Lambda, \Sigma \Sigma \rightarrow \Xi N, \Sigma \Lambda, \Sigma \Sigma), \\ I = 2 : & \Sigma \Sigma \rightarrow \Sigma \Sigma. \end{aligned} \quad (2.3)$$

$$V(q=0) = \begin{pmatrix} V_{aa} & \sqrt{\frac{1}{2}}V_{ba} & -\sqrt{\frac{1}{2}}V_{ba} & 0 & -\sqrt{\frac{1}{3}}V_{ad} & \sqrt{\frac{1}{3}}V_{ad} \\ \cdot & \frac{1}{2}[V_{bb}(1) + V_{bb}(0)] & \frac{1}{2}[V_{bb}(1) - V_{bb}(0)] & \sqrt{\frac{1}{2}}V_{bc} & -\sqrt{\frac{1}{6}}V_{bd}(0) & \sqrt{\frac{1}{6}}V_{bd}(0) - \frac{1}{2}V_{bd}(1) \\ \cdot & \cdot & \frac{1}{2}[V_{bb}(1) + V_{bb}(0)] & \sqrt{\frac{1}{2}}V_{bc} & \sqrt{\frac{1}{6}}V_{bd}(0) & -\sqrt{\frac{1}{6}}V_{bd}(0) - \frac{1}{2}V_{bd}(1) \\ \cdot & \cdot & \cdot & V_{cc} & 0 & -\sqrt{\frac{1}{2}}V_{cd} \\ \cdot & \cdot & \cdot & \cdot & \frac{1}{3}[2V_{dd}(2) + V_{dd}(0)] & \frac{1}{3}[V_{dd}(2) - V_{dd}(0)] \\ \cdot & \cdot & \cdot & \cdot & \cdot & \frac{1}{6}[V_{dd}(2) + 3V_{dd}(1) + 2V_{dd}(0)] \end{pmatrix}, \quad (2.5)$$

and for  $q = +1$  we have

$$V(q=+1) = \begin{pmatrix} V_{bb}(1) & V_{bc} & -\sqrt{\frac{1}{2}}V_{bd} \\ V_{bc} & V_{cc} & -\sqrt{\frac{1}{2}}V_{cd} \\ -\sqrt{\frac{1}{2}}V_{bd}(1) & -\sqrt{\frac{1}{2}}V_{cd} & \frac{1}{2}[V_{dd}(1) + V_{dd}(2)] \end{pmatrix}, \quad (2.6)$$

Here, when necessary an isospin label is added in parentheses.

The momentum space and configuration space potentials for the ESC-model have been described in [3] for baryon-baryon in general. Therefore, they apply also to

For the kinematics of the reactions and the various thresholds, see [14]. In this work we do not solve the Lippmann-Schwinger equation, but the multi-channel Schrödinger equation in configuration space, completely analogous to [15]. The multi-channel Schrödinger equation for the configuration-space potential is derived from the Lippmann-Schwinger equation through the standard Fourier transform, and the equation for the radial wave function is found to be of the form [15]

$$u''_{l,j} + (p_i^2 \delta_{i,j} - A_{i,j}) u_{l,j} - B_{i,j} u'_{l,j} = 0, \quad (2.4)$$

where  $A_{i,j}$  contains the potential, nonlocal contributions, and the centrifugal barrier, while  $B_{i,j}$  is only present when non-local contributions are included. The solution in the presence of open and closed channels is given, for example, in Ref. [21]. The inclusion of the Coulomb interaction in the configuration-space equation is well known and included in the evaluation of the scattering matrix.

Obviously, the potential on the particle basis for the  $q = 2$  and  $q = -2$  channels are given by the  $I = 2$   $\Sigma \Sigma$  potential on the isospin basis. For  $q = 0$  and  $q = \pm 1$ , the potentials are related to the potentials on the isospin basis by an isospin rotation. Using the indices  $a, b, c, d$  for  $\Lambda\Lambda, \Xi N, \Sigma \Lambda$ , and  $\Sigma \Sigma$  respectively, we have [22]

$$V(q=+1) = \begin{pmatrix} V_{bb}(1) & V_{bc} & -\sqrt{\frac{1}{2}}V_{bd} \\ V_{bc} & V_{cc} & -\sqrt{\frac{1}{2}}V_{cd} \\ -\sqrt{\frac{1}{2}}V_{bd}(1) & -\sqrt{\frac{1}{2}}V_{cd} & \frac{1}{2}[V_{dd}(1) + V_{dd}(2)] \end{pmatrix}, \quad (2.6)$$

hyperon-nucleon and we can refer for that part of the potential to paper I. Also in the ESC-model, the potentials are of such a form that they are exactly equivalent in both momentum space and configuration space. The treatment of the mass differences among the baryons

are handled exactly similar as is done in [14, 15]. Also, exchange potentials related to strange meson exchanges  $K, K^*$  etc., can be found in these references.

The baryon mass differences in the intermediate states for TME- and MPE- potentials has been neglected for  $YN$ -scattering. This, although possible in principle, becomes rather laborious and is not expected to change the characteristics of the baryon-baryon potentials.

### B. Potentials and SU(3) Symmetry

We consider all possible baryon-baryon interaction channels, where the baryons are the members of the  $J^P = \frac{1}{2}^+$  baryon octet

$$B = \begin{pmatrix} \frac{\Sigma^0}{\sqrt{2}} + \frac{\Lambda}{\sqrt{6}} & \Sigma^+ & p \\ \Sigma^- & -\frac{\Sigma^0}{\sqrt{2}} + \frac{\Lambda}{\sqrt{6}} & n \\ -\Xi^- & \Xi^0 & -\frac{2\Lambda}{\sqrt{6}} \end{pmatrix}. \quad (2.7)$$

The baryon masses, used in this paper, are given in Table V. The meson nonets can be written as

$$P = P_{\text{sin}} + P_{\text{oct}}, \quad (2.8)$$

where the singlet matrix  $P_{\text{sin}}$  has elements  $\eta_0/\sqrt{3}$  on the diagonal, and the octet matrix  $P_{\text{oct}}$  is given by

$$P_{\text{oct}} = \begin{pmatrix} \frac{\pi^0}{\sqrt{2}} + \frac{\eta_8}{\sqrt{6}} & \pi^+ & K^+ \\ \pi^- & -\frac{\pi^0}{\sqrt{2}} + \frac{\eta_8}{\sqrt{6}} & K^0 \\ K^- & \overline{K^0} & -\frac{2\eta_8}{\sqrt{6}} \end{pmatrix}, \quad (2.9)$$

and where we took the pseudoscalar mesons with  $J^P = 0^+$  as a specific example. For the other mesons the octet matrix is obtained by the following substitutions: (i) vector mesons  $\pi \rightarrow \rho$ ,  $\eta_8 \rightarrow \phi_8$ ,  $K \rightarrow K^*$ , (ii) scalar  $\pi \rightarrow a_0$ ,  $\eta_8 \rightarrow f_{0,8}$ ,  $K \rightarrow \kappa$ , (iii) axial-vector  $\pi \rightarrow A_1$ ,  $\eta_8 \rightarrow E_{1,8}$ ,  $K \rightarrow K_A$ .

Introducing the following notation for the isodoublets,

$$N = \begin{pmatrix} p \\ n \end{pmatrix}, \quad \Xi = \begin{pmatrix} \Xi^0 \\ \Xi^- \end{pmatrix}, \quad \text{and} \quad K = \begin{pmatrix} K^+ \\ K^0 \end{pmatrix}, \quad K_c = \begin{pmatrix} \overline{K^0} \\ -K^- \end{pmatrix}, \quad (2.10)$$

the most general, SU(3) invariant, interaction Hamiltonian is then given by [23]

$$\begin{aligned} \mathcal{H}_{\text{pv}}^{\text{oct}} = & g_{NN\pi}(\overline{N}\boldsymbol{\tau}N)\cdot\boldsymbol{\pi} - ig_{\Sigma\Sigma\pi}(\overline{\Sigma}\times\Sigma)\cdot\boldsymbol{\pi} + g_{\Lambda\Sigma\pi}(\overline{\Lambda}\Sigma + \overline{\Sigma}\Lambda)\cdot\boldsymbol{\pi} + g_{\Xi\Sigma\pi}(\overline{\Xi}\boldsymbol{\tau}\Xi)\cdot\boldsymbol{\pi} + \\ & g_{\Lambda NK}[(\overline{N}K)\Lambda + \overline{\Lambda}(\overline{K}N)] + g_{\Xi\Lambda K}[(\overline{\Xi}K_c)\Lambda + \overline{\Lambda}(\overline{K}_c\Xi)] + \\ & g_{\Sigma NK}[\overline{\Sigma}\cdot(\overline{K}\boldsymbol{\tau}N) + (\overline{N}\boldsymbol{\tau}K)\cdot\Sigma] + g_{\Xi\Sigma K}[\overline{\Sigma}\cdot(\overline{K}_c\boldsymbol{\tau}\Xi) + (\overline{\Xi}\boldsymbol{\tau}K_c)\cdot\Sigma] + \\ & g_{NN\eta_8}(\overline{N}N)\eta_8 + g_{\Lambda\Lambda\eta_8}(\overline{\Lambda}\Lambda)\eta_8 + g_{\Sigma\Sigma\eta_8}(\overline{\Sigma}\cdot\Sigma)\eta_8 + g_{\Xi\Xi\eta_8}(\overline{\Xi}\Xi)\eta_8 + \\ & g_{NN\eta_0}(\overline{N}N)\eta_0 + g_{\Lambda\Lambda\eta_0}(\overline{\Lambda}\Lambda)\eta_0 + g_{\Sigma\Sigma\eta_0}(\overline{\Sigma}\cdot\Sigma)\eta_0 + g_{\Xi\Xi\eta_0}(\overline{\Xi}\Xi)\eta_0, \end{aligned} \quad (2.11)$$

where we again took the pseudoscalar mesons as an example, dropped the Lorentz character of the interaction vertices, and introduced the charged-pion mass to make the pseudovector coupling constant  $f$  dimensionless. All coupling constants can be expressed in terms of only four parameters. The explicit expressions can be found in Ref. [14]. The  $\Sigma$ -hyperon is an isovector with phase chosen such [23] that

$$\Sigma\cdot\boldsymbol{\pi} = \Sigma^+\pi^- + \Sigma^0\pi^0 + \Sigma^-\pi^+. \quad (2.12)$$

This definition for  $\Sigma^+$  differs from the standard Condon and Shortley phase convention [24] by a minus sign. This means that, in working out the isospin multiplet

for each coupling constant in Eq. (2.11), each  $\Sigma^+$  entering or leaving an interaction vertex has to be assigned an extra minus sign. However, if the potential is first evaluated on the isospin basis and then, via an isospin rotation, transformed to the potential on the physical particle basis (see below), this extra minus sign will be automatically accounted for.

In appendix A, Table XVI and Table XVII we give the relation between the potentials on the isospin-basis, see (2.5)-(2.6), and the SU(3)-irreps.

Given the interaction Hamiltonian (2.11) and a theoretical scheme for deriving the potential representing a particular Feynman diagram, it is now straightforward

to derive the one-meson-exchange baryon-baryon potentials. We follow the Thompson approach [25–28] and expressions for the potential in momentum space can be found in Ref. [15]. Since the nucleons have strangeness  $S = 0$ , the hyperons  $S = -1$ , and the cascades  $S = -2$ , the possible baryon-baryon interaction channels can be classified according to their total strangeness, ranging from  $S = 0$  for  $NN$  to  $S = -4$  for  $\Xi\Xi$ . Apart from the wealth of accurate  $NN$  scattering data for the total strangeness  $S = 0$  sector, there are only a few, and not very accurate,  $YN$  scattering data for the  $S = -1$  sector, while there are no data at all for the  $S < -1$  sectors. We therefore believe that at this stage it is not yet worthwhile to explicitly account for the small mass differences between the specific charge states of the baryons and mesons; i.e., we use average masses, isospin is a good quantum number, and the potentials are calculated on the isospin basis. The possible channels on the isospin basis are given in (2.3).

However, the Lippmann-Schwinger or Schrödinger equation is solved for the physical particle channels, and so scattering observables are calculated using the proper physical baryon masses. The possible channels on the physical particle basis can be classified according to the total charge  $Q$ ; these are given in (2.2). The corresponding potentials are obtained from the potential on the isospin basis by making the appropriate isospin rotation. The matrix elements of the isospin rotation matrices are nothing else but the Clebsch-Gordan coefficients for the two baryon isospins making up the total isospin. (Note that this is the reason why the potential on the particle basis, obtained from applying an isospin rotation to the potential on the isospin basis, will have the correct sign for any coupling constant on a vertex which involves a  $\Sigma^+$ .)

In order to construct the potentials on the isospin basis, we need first the matrix elements of the various OBE exchanges between particular isospin states. Using the iso-multiplets (2.9) and the Hamiltonian (2.11) the isospin factors can be calculated. The results are given in Table I, where we use the pseudoscalar mesons as a specific example. The entries contain the flavor-exchange operator  $P_f$ , which is  $+1$  for a flavor symmetric and  $-1$  for a flavor anti-symmetric two-baryon state. Since two-baryons states are totally anti-symmetric, one has  $P_f = -P_x P_\sigma$ . Therefore, the exchange operator  $P_f$  has the value  $P_f = +1$  for even- $L$  singlet and odd- $L$  triplet partial waves, and  $P_f = -1$  for odd- $L$  singlet and even- $L$  triplet partial waves. In order to understand Table I fully, we have given in the following section Sec. III a general treatment of exchange forces. This treatment shows also how to deal with the case where the initial/final state involves identical particles and the final/initon state does not.

Second, we need to evaluate the TME and the MPE exchanges. The method we used for these is the same as for hyperon-nucleon, and is described in [4], Sec. IID.

### III. EXCHANGE FORCES

The proper treatment of the flavor-exchange forces is for the  $S \leq -2$ -channels more difficult than for the

$S = 0, -1$ -channels. The extra complication is the occurrence of couplings between channels with identical and channels with non-identical particles. In order to understand the several  $\sqrt{2}$ -factors, see [7], we give here a systematic treatment of the flavor-exchange potentials. The method followed is using a multi-channel framework, which starts by ordering the two-particle states by assigning  $A_i$  and  $B_i$  for the channel labeled with the index  $i$ , like in eq. (2.1). The particles  $A_i$  and  $B_i$  have CM-momenta  $p_i$  and  $-p_i$ , spin components  $s_{A,i}$  and  $s_{B,i}$ . The two-baryon states  $|A_i B_i\rangle$  and  $|B_i A_i\rangle$  are considered to be distinct, leading to distinct two-baryon channels. The 'direct' and the 'exchange' T-amplitudes are given by the T-matrix elements

$$\langle A_j B_j | T_d | A_i B_i \rangle, \quad \langle B_j A_j | T_e | A_i B_i \rangle, \quad (3.1)$$

and similarly for the direct and flavor-exchange potentials  $V_d$  and  $V_e$ . It is obvious from rotation invariance that

$$\begin{aligned} \langle A_j B_j | T_d | A_i B_i \rangle &= \langle B_j A_j | T_d | B_i A_i \rangle, \\ \langle B_j A_j | T_e | A_i B_i \rangle &= \langle A_j B_j | T_e | B_i A_i \rangle. \end{aligned} \quad (3.2)$$

A similar definition (3.1) and relation (3.2) apply for the direct and flavor-exchange potentials  $V_d$  and  $V_e$ . We no-

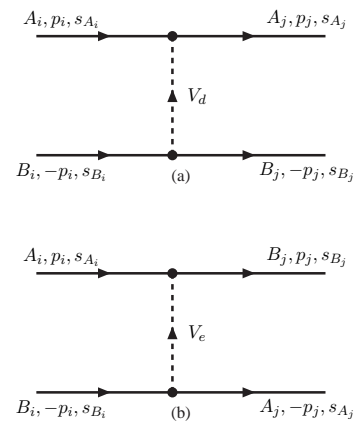


FIG. 2:  $V_d$  (a) and  $V_e$  (b) in CM-system.

ice that in interchanging A and B there is no exchange of momenta or spin-components, see Fig. 2. This is necessary for the application of Lippmann-Schwinger type of integral equations, which can produce only one type of spectral function e.g.  $\rho(s, t)$ . So, the momentum transfer for  $V_d$  and for  $V_e$  is the same. Viewed from the coupled-channel scheme this is the standard situation.

The integral equations with two-baryon unitarity, e.g. the Thompson-, Lippmann-Schwinger-equation etc., read for the  $T_d$ - and  $T_e$ -operator

$$\begin{aligned} \langle A_j B_j | T_d | A_i B_i \rangle &= \langle A_j B_j | V_d | A_i B_i \rangle + \sum_k [\langle A_j B_j | V_d | A_k B_k \rangle G_k \langle A_k B_k | T_d | A_i B_i \rangle \\ &\quad + \langle A_j B_j | V_e | B_k A_k \rangle G_k \langle B_k A_k | T_e | A_i B_i \rangle] , \end{aligned} \quad (3.3a)$$

$$\begin{aligned} \langle B_j A_j | T_e | A_i B_i \rangle &= \langle B_j A_j | V_e | A_i B_i \rangle + \sum_k [\langle B_j A_j | V_d | B_k A_k \rangle G_k \langle B_k A_k | T_e | A_i B_i \rangle \\ &\quad + \langle B_j A_j | V_e | A_k B_k \rangle G_k \langle A_k B_k | T_d | A_i B_i \rangle] . \end{aligned} \quad (3.3b)$$

These coupled equations can be diagonalized by introducing the  $T^\pm$ - and  $V^\pm$ -operators

$$T^\pm = T_d \pm T_e , \quad V^\pm = V_d \pm V_e . \quad (3.4)$$

which, as follows from (3.3), satisfy separate integral equations

$$\begin{aligned} \langle A_j B_j | T^\pm | A_i B_i \rangle &= \langle A_j B_j | V^\pm | A_i B_i \rangle + \\ &\quad \sum_k \langle A_j B_j | V^\pm | A_k B_k \rangle G_k \langle A_k B_k | T^\pm | A_i B_i \rangle . \end{aligned} \quad (3.5)$$

Notice that on the basis of states with definite flavor symmetry

$$|A_i B_i\rangle_\pm = \frac{1}{\sqrt{2}} [|A_i B_i\rangle \pm |B_i A_i\rangle] , \quad (3.6)$$

the  $T^\pm$  and  $V^\pm$  matrix elements are also given by

$$T_{ij}^\pm = \pm \langle A_i B_i | T | A_j B_j \rangle_\pm , \quad V_{ij}^\pm = \pm \langle A_i B_i | V | A_j B_j \rangle_\pm . \quad (3.7)$$

### A. Identical Particles

Sofar, we considered the general case where  $A_i \neq B_i$  for all channels. In the case that  $A_i = B_i$  for some  $i$ , one has  $\langle B_i A_i | V_e | A_i B_i \rangle = 0$ , because there is no distinct physical state corresponding to the 'flavor exchange-state'. For example for a flavor single channel like  $pp$  one deduces from (3.3) that then also  $T_e = 0$ , and one has in this case the integral equation

$$\begin{aligned} \langle A_j B_j | T_d | A_i B_i \rangle &= \langle A_j B_j | V_d | A_i B_i \rangle + \\ &\quad \sum_k \langle A_j B_j | V_d | A_k B_k \rangle G_k \langle A_k B_k | T_d | A_i B_i \rangle , \end{aligned} \quad (3.8)$$

$$\begin{pmatrix} \Lambda\Lambda \\ \Xi N \\ N\Xi \end{pmatrix} \Rightarrow \begin{pmatrix} \Lambda\Lambda \\ (\Xi N + N\Xi)/\sqrt{2} \\ (\Xi N - N\Xi)/\sqrt{2} \end{pmatrix} = \begin{pmatrix} 1 & 0 & 0 \\ 0 & 1/\sqrt{2} & 1/\sqrt{2} \\ 0 & 1/\sqrt{2} & -1/\sqrt{2} \end{pmatrix} \begin{pmatrix} \Lambda\Lambda \\ \Xi N \\ N\Xi \end{pmatrix} . \quad (3.11)$$

one gets in the transformed basis for the potential

$$UVU^{-1} = \begin{pmatrix} V_{\Lambda\Lambda;\Lambda\Lambda} & (V_{\Lambda\Lambda;\Xi N} + V_{\Lambda\Lambda;N\Xi})/\sqrt{2} & (V_{\Lambda\Lambda;\Xi N} - V_{\Lambda\Lambda;N\Xi})/\sqrt{2} \\ (V_{\Xi N;\Lambda\Lambda} + V_{N\Xi;\Lambda\Lambda})/\sqrt{2} & (V_{\Xi N;\Xi N} + V_{\Xi N;N\Xi}) & 0 \\ (V_{\Xi N;\Lambda\Lambda} - V_{N\Xi;\Lambda\Lambda})/\sqrt{2} & 0 & (V_{\Xi N;\Xi N} - V_{\Xi N;N\Xi}) \end{pmatrix} , \quad (3.12)$$

and of course, a similar form is obtained for the T-matrix on the transformed basis.

Now, obviously we have that  $V_{\Lambda\Lambda;\Xi N} = V_{\Lambda\Lambda;N\Xi}$  and  $V_{\Xi N;\Lambda\Lambda} = V_{N\Xi;\Lambda\Lambda}$ . Therefore, one sees that the even

where the labels  $i$  and  $j$  now denote e.g. the spin-components.

### B. Coupled $\Lambda\Lambda$ and $\Xi N$ system

This multi-channel system represents the case where there is mixture of channels with identical and with non-identical particles. The three states we distinguish are  $|\Lambda\Lambda\rangle$ ,  $|\Xi N\rangle$ , and  $|N\Xi\rangle$ . Choosing the same ordering, the potential written as a  $3 \times 3$ -matrix reads

$$V = \begin{pmatrix} (\Lambda\Lambda|V|\Lambda\Lambda) & (\Lambda\Lambda|V|\Xi N) & (\Lambda\Lambda|V|N\Xi) \\ (\Xi N|V|\Lambda\Lambda) & (\Xi N|V|\Xi N) & (\Xi N|V|N\Xi) \\ (N\Xi|V|\Lambda\Lambda) & (N\Xi|V|\Xi N) & (N\Xi|V|N\Xi) \end{pmatrix} . \quad (3.9)$$

With a similar notation for the T-matrix, the Lippmann-Schwinger equation can be written compactly as a  $3 \times 3$ -matrix equation:

$$T = V + V G T , \quad \text{with } G_{ij} = G_i \delta_{ij} . \quad (3.10)$$

Next, we make a transformation to states, which are either symmetric or anti-symmetric for particle interchange. Then, according to the discussion above, we can separate them in the Lippmann-Schwinger equation. This is achieved by the transformation

$$\begin{pmatrix} \Lambda\Lambda \\ \Xi N \\ N\Xi \end{pmatrix} \Rightarrow \begin{pmatrix} \Lambda\Lambda \\ (\Xi N + N\Xi)/\sqrt{2} \\ (\Xi N - N\Xi)/\sqrt{2} \end{pmatrix} = \begin{pmatrix} 1 & 0 & 0 \\ 0 & 1/\sqrt{2} & 1/\sqrt{2} \\ 0 & 1/\sqrt{2} & -1/\sqrt{2} \end{pmatrix} \begin{pmatrix} \Lambda\Lambda \\ \Xi N \\ N\Xi \end{pmatrix} . \quad (3.11)$$

and odd states under particle exchange are decoupled in (3.12). Also  $(V_{\Xi N; \Lambda\Lambda} + V_{N\Xi; \Lambda\Lambda})/\sqrt{2} = \sqrt{2}V_{\Xi N; \Lambda\Lambda}$ , etc. showing the appearance of the  $\sqrt{2}$ -factors, mentioned before. Indeed, they appear in a systematic way using the multi-channel framework.

### C. The K-exchange Potentials

Consider for example the  $(\Lambda\Lambda, \Xi N)$ -system, having  $I = 0$ . Mesons with strangeness, i.e.  $K(495)$ ,  $K^*(892)$ ,  $\kappa(841)$ ,  $K_A(1273)$ ,  $K_B(1400)$ , are obviously the only ones that can give transition potentials, i.e.  $V_{\Lambda\Lambda; \Xi N} \neq 0$  and  $V_{\Xi N; \Lambda\Lambda} \neq 0$ . The  $\Xi N$  ( $I = 0$ )-states anti-symmetric and symmetric in flavor are respectively:

$$P_f = -1 : \frac{1}{\sqrt{2}} [|\Xi N(I=0)\rangle - |N\Xi(I=0)\rangle] \quad (3.13a)$$

$$P_f = +1 : \frac{1}{\sqrt{2}} [|\Xi N(I=0)\rangle + |N\Xi(I=0)\rangle] \quad (3.13b)$$

Analyzing the  $^1S_0$ -state one has because of the anti-symmetry of the two-fermion state w.r.t. the exchange of all quantum labels,  $P_f = -P_\sigma P_x = +1$ , where  $P_f$  denotes the flavor-symmetry. Taking here the  $K(495)$  as a generic example, and using (2.10) and (2.11), one finds that

$$\langle \Xi^0 n | V(K) | \Lambda\Lambda \rangle = +g_{K\Lambda N} g_{K\Xi\Lambda}, \quad (3.14)$$

$$\langle \Xi^- p | V(K) | \Lambda\Lambda \rangle = -g_{K\Lambda N} g_{K\Xi\Lambda}. \quad (3.15)$$

Then, since  $|\Xi N(I=0)\rangle = [|\Xi^0 n\rangle - |\Xi^- p\rangle]/\sqrt{2}$ , one obtains for the 'direct' potential the coupling

$$V_{\Xi N; \Lambda\Lambda} = \langle \Xi N(I=0) | V_d(K) | \Lambda\Lambda \rangle \Leftarrow \sqrt{2}g_{K\Lambda N} g_{K\Xi\Lambda}. \quad (3.16)$$

The same result is found for the 'exchange' potential  $V_{N\Xi; \Lambda\Lambda}$ . Therefore

$$\frac{1}{\sqrt{2}} (V_{\Xi N; \Lambda\Lambda} + V_{N\Xi; \Lambda\Lambda}) = \langle \Xi N(I=0) | V(K) | \Lambda\Lambda \rangle \Leftarrow 2g_{K\Lambda N} g_{K\Xi\Lambda}, \quad (3.17)$$

which has indeed the  $(1+P_f)$ -factor given in Table I, and is identical to Table IV in [7], for  $(\Lambda\Lambda|K|\Xi N)$ .

For  $\langle \Xi N|K|\Sigma\Lambda \rangle$  the entry for  $I = 1$  consists of two parts. These correspond to  $V_d \propto g_{\Lambda N K} g_{\Xi \Sigma K}$  and  $V_e \propto g_{\Sigma N K} g_{\Xi \Lambda K}$  respectively, i.e. the direct and exchange contributions involve different couplings. Therefore, they are not added together.

### D. The $\eta$ - and $\pi$ -exchange Potentials

Next, we discuss briefly the calculation of the entries for  $\eta$ - and  $\pi$ -exchange in Table I. First, the entries with  $\text{—}$  indicate that the corresponding physical state does not exist. Next we give further specific remarks and calculations:

TABLE I: Isospin factors for the various meson exchanges in the different total strangeness and isospin channels.  $P_f$  is the flavor-exchange operator. The  $I = 2$  case only contributes to  $S = -2$   $\Sigma\Sigma$  scattering, where the isospin factors can collectively be given by  $(\Sigma\Sigma|\eta, \eta', \pi|\Sigma\Sigma) = \frac{1}{2}(1+P_f)$ , and so they are not separately displayed in the table. Non-existing channels are marked by a long-dash.

$S = -2$	$I = 0$	$I = 1$
$(\Lambda\Lambda \eta, \eta' \Lambda\Lambda)$	$\frac{1}{2}(1+P_f)$	—
$(\Xi N \eta, \eta' \Xi N)$	$\frac{1}{2}(1+P_f)$	1
$(\Sigma\Sigma \eta, \eta' \Sigma\Sigma)$	$\frac{1}{2}(1+P_f)$	$\frac{1}{2}(1-P_f)$
$(\Sigma\Lambda \eta, \eta' \Sigma\Lambda)$	—	1
$(\Xi N \pi \Xi N)$	-3	1
$(\Sigma N \pi \Sigma\Sigma)$	$-(1+P_f)$	$-\frac{1}{2}(1-P_f)$
$(\Lambda\Lambda \pi \Sigma\Sigma)$	$-\frac{1}{2}\sqrt{3}(1+P_f)$	—
$(\Sigma\Lambda \pi \Lambda\Sigma)$	—	$P_f$
$(\Sigma\Sigma \pi \Sigma\Lambda)$	—	$(1-P_f)$
$(\Lambda\Lambda K \Xi N)$	$1+P_f$	—
$(\Sigma\Sigma K \Xi N)$	$\sqrt{3}(1+P_f)$	$\sqrt{2}(1-P_f)$
$(\Xi N K \Sigma\Lambda)$	—	$\sqrt{2}; -P_f \sqrt{2}$

- a. For  $\eta, \eta'$ -exchange one has that  $V_e = 0$ . The matrix elements for the  $\Lambda\Lambda$ - and  $\Xi N$ -state are easily seen to be correct. For the  $\Sigma\Sigma$ -states one has  $P_f = 1$  for  $I_{\Sigma\Sigma} = 0, 2$ , and  $P_f = -1$  for  $I_{\Sigma\Sigma} = 1$ . This explains the  $\Sigma\Sigma$  matrix element.
- b. For  $\langle \Xi N|\pi|\Xi N \rangle$  the calculation is identical to that for NN, in particular  $pn$ .
- c. For  $\langle \Sigma\Sigma|\pi|\Sigma\Sigma \rangle$  consider the  $I = 0, I_3 = 0$  and  $I = 1, I_3 = 0$  matrix elements. In these cases one has  $V_e = 0$  as one can easily check. Then, using the cartesian base, we have for  $\langle \Sigma_i \Sigma_m | \pi | \Sigma_j \Sigma_n \rangle \Rightarrow -g_{\Sigma\Sigma\pi}^2 \sum_{p=1}^3 \epsilon_{jip} \epsilon_{nmp} = -g_{\Sigma\Sigma\pi}^2 (\delta_{jn} \delta_{im} - \delta_{jm} \delta_{in})$ . Employing the states  $|I = 0, I_3 = 0\rangle \sim -\sum_{i,m=1}^3 \delta_{im} |\Sigma_i \Sigma_m\rangle/\sqrt{3}$  and  $|I = 1, I_3 = 0\rangle \sim -i \sum_{i,m=1}^3 \epsilon_{im3} |\Sigma_i \Sigma_m\rangle/\sqrt{2}$ , one obtains the results in Table I.

With the ingredients given above one can easily check the other entries in Table I.

## IV. SHORT-RANGE PHENOMENOLOGY

For a detailed discussion and description of the short-range region we refer to paper II [2]. Here, the meson- and diffractive-exchange and the quark-core in the ESC08c-modeling has been described. In this section we give the quark-core phenomenology for the  $S=-2$  baryon-baryon channels.

### A. Relation S=-2 YN,YY-states and $SU_{fs}(6)$ -irreps

The relation between the  $SU_f(3)$ -irreps and  $SU_{fs}(6)$ -irreps has been derived in paper II [2]. In Appendix A the S=-2 BB-potentials are given in terms of the  $SU(3)_f$ -irreps. Combining these two things gives the representation of the S=-2 potentials in terms of the  $SU_{fs}(6)$ -irreps as displayed in Tables IV A and IV A.

TABLE II:  $SU(6)_{fs}$ -contents spin-space odd  $^1S_0, ^3P, ^1D_2, \dots$  potentials on the spin-isospin basis.

	$(S, I)$	$V = aV_{[51]} + bV_{[33]}$
$\Lambda\Lambda \rightarrow \Lambda\Lambda$	(0, 0)	$V_{\Lambda\Lambda, \Lambda\Lambda} = \frac{1}{2}V_{[51]} + \frac{1}{2}V_{[33]}$
$\Xi N \rightarrow \Xi N$	(0, 0)	$V_{\Xi N, \Xi N} = \frac{1}{3}V_{[51]} + \frac{2}{3}V_{[33]}$
$\Sigma\Sigma \rightarrow \Sigma\Sigma$	(0, 0)	$V_{\Sigma\Sigma, \Sigma\Sigma} = \frac{11}{18}V_{[51]} + \frac{7}{18}V_{[33]}$
$\Xi N \rightarrow \Xi N$	(0, 1)	$V_{\Xi N, \Xi N} = \frac{7}{9}V_{[51]} + \frac{2}{9}V_{[33]}$
$\Sigma\Lambda \rightarrow \Sigma\Lambda$	(0, 1)	$V_{\Sigma\Lambda, \Sigma\Lambda} = \frac{2}{3}V_{[51]} + \frac{1}{3}V_{[33]}$
$\Sigma\Sigma \rightarrow \Sigma\Sigma$	(0, 2)	$V_{\Sigma\Sigma, \Sigma\Sigma} = \frac{4}{9}V_{[51]} + \frac{5}{9}V_{[33]}$

TABLE III:  $SU(6)_{fs}$ -contents of the spin-space even  $^3S_1, ^1P_1, ^3D, \dots$  potentials on the spin-isospin basis.

	$(S, I)$	$V = aV_{[51]} + bV_{[33]}$
$\Xi N \rightarrow \Xi N$	(1, 0)	$V_{\Xi N, \Xi N} = \frac{5}{9}V_{[51]} + \frac{4}{9}V_{[33]}$
$\Xi N \rightarrow \Xi N$	(1, 1)	$V_{\Xi N, \Xi N} = \frac{17}{27}V_{[51]} + \frac{10}{27}V_{[33]}$
$\Sigma\Lambda \rightarrow \Sigma\Lambda$	(1, 1)	$V_{\Sigma\Lambda, \Sigma\Lambda} = \frac{2}{3}V_{[51]} + \frac{1}{3}V_{[33]}$
$\Sigma\Sigma \rightarrow \Sigma\Sigma$	(1, 1)	$V_{\Sigma\Sigma, \Sigma\Sigma} = \frac{16}{27}V_{[51]} + \frac{11}{27}V_{[33]}$

### B. Parametrization Quark-core effects

As introduced in II, the repulsive short-range Pomeron-like YN,YY potential is splitted linearly in a diffractive (Pomeron) and a quark-core component by writing

$$V_{BB} = V_{BB}(POM) + V_{BB}(PB) \quad (4.1)$$

where  $V_{BB}(POM)$  represents the genuine Pomeron and  $V_{BB}(PB)$  the structural effects of the quark-core forbidden [51]-configuration, i.e. a Pauli-blocking (PB) effect. Since the Pomeron is a unitary-singlet its contribution is the same for all BB-channels (apart from some

TABLE IV: Effective Pomeron+PB contribution on the spin,isospin basis.

	$(S, I)$	$V_{PBB}/V_{PN}$	$ESC08c$
$NN \rightarrow NN$	(0, 1)	1	1.000
$NN \rightarrow NN$	(1, 0)	1	1.000
$\Lambda\Lambda \rightarrow \Lambda\Lambda$	(0, 0)	$1 + \frac{1}{8}a_{PB}$	1.034
$\Xi N \rightarrow \Xi N$	(0, 0)	$1 - \frac{1}{4}a_{PB}$	0.931
$\Sigma\Sigma \rightarrow \Sigma\Sigma$	(0, 0)	$1 + \frac{3}{8}a_{PB}$	1.103
$\Xi N \rightarrow \Xi N$	(0, 1)	$1 + \frac{3}{4}a_{PB}$	1.206
$\Sigma\Lambda \rightarrow \Sigma\Lambda$	(0, 1)	$1 + \frac{1}{2}a_{PB}$	1.138
$\Sigma\Sigma \rightarrow \Sigma\Sigma$	(0, 2)	1	1.000
$\Xi N \rightarrow \Xi N$	(1, 0)	$1 + \frac{1}{4}a_{PB}$	1.069
$\Xi N \rightarrow \Xi N$	(1, 1)	$1 + \frac{5}{12}a_{PB}$	1.115
$\Sigma\Lambda \rightarrow \Sigma\Lambda$	(1, 1)	$1 + \frac{1}{2}a_{PB}$	1.138
$\Sigma\Sigma \rightarrow \Sigma\Sigma$	(1, 1)	$1 + \frac{1}{3}a_{PB}$	1.092

small baryon mass breaking effects), i.e.  $V_{BB}(POM) = V_{NN}(POM)$ . Furthermore the PB-effect for the BB-channels is assumed to be proportional to the relative weight of the forbidden [51]-configuration compared to its weight in NN

$$V_{BB}(PB) = a_{PB} (w_{BB}[51]/w_{NN}[51]) \cdot V_{NN}(PB) \quad (4.2)$$

where  $a_{PB}$  denotes the quark-core fraction w.r.t. the pomeron potential for the NN-channel, i.e.  $V_{NN}(PB) = a_{PB} V_{PN}$ . Then we have

$$V_{PBB} = (1 - a_{PB})V_{PN} + a_{PB} \left( \frac{w_{BB}[51]}{w_{NN}[51]} \right) \cdot V_{PN} \quad (4.3)$$

A subtle treatment of *all* BB channels according to this linear scheme is characteristic for the ESC08c-model. The value of the PB factor  $a_{PB}$  is searched in the fit to the NN- and YN-data. The parameter  $a_{PB}$  turns out to be about 27.5%. This means that the Quark-core repulsion is roughly 34% of the genuine Pomeron repulsion. Then, the PB effects in the S=-2 channels are entirely determined. From Eqn. (4.3) the ratio  $V_{PBB}/V_{PN}$  is given by the weights of the [51]-irrep and  $a_{PB}$ . In Table IV B we give this ratio for the various S=-2 BB channels in the ESC08c model. With only one exception, the effective pomeron repulsion is stronger than in the NN-channels.

## V. MULTI-CHANNEL THRESHOLDS AND POTENTIALS

### A. Thresholds

Clearly, the  $S = -2$  two-baryon channels represent a number of separate coupled-channel systems, separated by the charge, see (2.2). A further subdivision is according to the total isospin. The different thresholds have been discussed in detail in [7], and we show these thresholds here in Fig. 1 for the purpose of general orientation. Their presence turns the Lippmann-Schwinger and Schrödinger equation into a coupled-channel matrix equation, where the different channels open up at different energies. In general one has a combination of 'open' and 'closed' channels. For a discussion of the solution of such a mixed system, we refer to [29].

### B. Threshold- and Meson-mass corrections in Potentials

As discussed in [7], the one-meson-exchange Feynman-graph consists actually of two three-dimensional time-ordered graphs. The energy denominator from these two diagrams reads

$$D(\omega) = \frac{1}{2\omega} \left[ \frac{1}{E_2 + E_3 - W + \omega} + \frac{1}{E_1 + E_4 - W + \omega} \right], \quad (5.1)$$

where,  $W = \sqrt{s}$  is the total energy and  $\omega^2 = \mathbf{k}^2 + m^2$ , with  $m$  the meson mass and  $\mathbf{k} = \mathbf{p}' - \mathbf{p}$  the momentum transfer. From (5.1) it is clear that the potential is energy dependent. We use the static approximation  $E_i \rightarrow M_i$  and  $W \rightarrow M_1^0 + M_2^0$ , where the superscript 0 refers to the masses of the lowest threshold of the particular coupled-channel system  $q$ , see (2.2). They are in general not equal to the masses  $M_1$  and  $M_2$  occurring in the time-ordered diagrams. For example, the potential for the  $\Sigma\Sigma$  contribution in the coupled-channel  $\Lambda\Lambda$  system has  $M_1 = M_2 = M_\Sigma$ , but  $M_1^0 = M_2^0 = M_\Lambda$ . Denoting  $a \equiv E_2 + E_3 - W \approx M_2 + M_3 - M_1^0 - M_2^0 > 0$ , and similarly for  $E_1 + E_4 - W$ , we have for the 'propagators' [27] for  $a > 0$

$$\frac{1}{\omega(\omega + a)} = \frac{2}{\pi} \int_0^\infty \frac{ad\lambda}{(a^2 + \lambda^2)(\omega^2 + \lambda^2)}. \quad (5.2)$$

For  $a < 0$  there is the extra term  $+2\theta(-a)/(\omega^2 - a^2)$  on the r.h.s. in (5.2). This integral representation makes it possible to deal with it numerically rather exactly. However, we think that such a sophistication is unnecessary at present nor for a description of the  $S = -1$  scattering data, nor for  $S = -2$ , where there are virtually no data at all. Therefore, we handle with this energy dependence approximately as follows:

1. Elastic potentials: In this case we use (5.2), and in (5.1) one has  $E_1 = E_3 \approx M_i$  and  $E_2 = E_4 \approx M'_i$ , for the

TABLE V: Baryon masses in  $\text{MeV}/c^2$ .

Baryon	Mass
Nucleon	$p$ 938.2796
	$n$ 939.5731
Hyperon	$\Lambda$ 1115.60
	$\Sigma^+$ 1189.37
	$\Sigma^0$ 1192.46
	$\Sigma^-$ 1197.436
Cascade	$\Xi^0$ 1314.90
	$\Xi^-$ 1321.32

elastic channel, label  $i$ . Here  $a \approx M_i + M'_i - M_1^0 - M_2^0 \geq 0$ . Then,

$$D_i(\omega) = \frac{1}{\omega^2} + \Delta_i(\omega, a), \quad \Delta_i(\omega, a) = \frac{2}{\pi} \int_0^\infty \frac{ad\lambda}{a^2 + \lambda^2} \times \left[ \frac{1}{\omega^2} - \frac{1}{\omega^2 + \lambda^2} \right], \quad (5.3)$$

for  $0 < a < m$ . Because of this condition we can not apply this to the pseudoscalars, but is possible for the vector-, scalar-, and axial-mesons. The largest effect is for  $\Lambda\Lambda$ -scattering, where the  $\Sigma\Sigma$ -channel potential is somewhat reduced by this effect. This because the  $\Sigma\Sigma$ -channel is rather far away from the others. In this paper we neglect the effects of a finite  $a$  in all elastic channels and for all mesons.

2. Inelastic potentials: In this case, like in [7] and all other papers on the Nijmegen potentials, we use the approximation of [30], using the fact that  $M_1^0 + M_2^0$  is mostly rather close to the average of the initial and final-state baryon masses. Then, the propagator can be written as

$$D(\omega) \rightarrow \frac{1}{\omega^2 - \frac{1}{4}(M_3 - M_4 + M_2 - M_1)^2}, \quad (5.4)$$

which amounts to introducing an effective meson mass  $\bar{m}$

$$m^2 \rightarrow \bar{m}^2 = m^2 - \frac{1}{4}(M_3 - M_4 + M_2 - M_1)^2. \quad (5.5)$$

For more details of this effect on the exchanged meson masses, we refer to [7].

The used baryon masses are about the same as in [7], and are given in Table V. The used meson masses are the same as in paper II [2], as well as the cut-off masses.

## VI. RESULTS

The main purpose of this paper is to present the properties of the ESC08c potentials for the  $S = -2$  sector. As described above, the free parameters in each model are fitted mainly to the  $NN$  and  $YN$  scattering data for the  $S = 0$  and  $S = -1$  sectors, respectively. Given the expressions for the coupling constants in terms of the

octet and singlet parameters and their values for the six different models as presented in Ref. [14], it is straightforward to evaluate all possible baryon-baryon-meson coupling constants needed for the  $S \leq -2$  potentials. A complete set of coupling constants for models ESC08c is

TABLE VI: Coupling constants for model ESC08c, divided by  $\sqrt{4\pi}$ .  $M$  refers to the meson. The coupling constants are listed in the order pseudoscalar, vector ( $g$  and  $f$ ), axial vector A ( $g$  and  $f$ ), scalar, axial vector B, and diffractive.

$M$	$NNM$	$\Sigma\Sigma M$	$\Sigma\Lambda M$	$\Xi\Xi M$	$M$	$\Lambda N M$	$\Lambda\Xi M$	$\Sigma N M$	$\Sigma\Xi M$
$f \ \pi$	0.2687	0.1961	0.1970	-0.0725	$K$	-0.2683	0.0714	0.0725	-0.2687
$g \ \rho$	0.6446	1.2892	0.0000	0.6446	$K^*$	-1.1165	1.1165	-0.6446	-0.6446
$f \ \rho$	3.7743	3.5639	2.3006	-0.2104		-4.2367	1.9362	0.2104	-3.7743
$g \ a_1$	-0.7895	-0.4929	-0.6271	0.2967	$K_{1A}$	0.7404	-0.1133	-0.2967	0.7895
$f \ a_1$	-0.8192	-0.5114	-0.6507	0.3078		0.7683	-0.1175	-0.3078	0.8192
$g \ a_0$	0.5852	1.1705	0.0000	0.5852	$\kappa$	-1.0137	1.0137	-0.5852	-0.5852
$f \ b_1$	-1.3743	-1.0991	-0.9523	0.2746	$K_{1B}$	1.4280	-0.4758	-0.2746	1.3743
$g \ a_2$	0.00000	0.00000	0.00000	0.00000	$K^{**}$	0.00000	0.00000	0.00000	0.00000
$M$	$NNM$	$\Lambda\Lambda M$	$\Sigma\Sigma M$	$\Xi\Xi M$	$M$	$NNM$	$\Lambda\Lambda M$	$\Sigma\Sigma M$	$\Xi\Xi M$
$f \ \eta$	0.1265	-0.1349	0.2490	-0.2045	$\eta'$	0.2309	0.2912	0.2026	0.3073
$g \ \omega$	3.4570	2.7589	2.7589	2.0608	$\phi$	-1.3390	-2.2103	-2.2103	-3.0816
$f \ \omega$	-0.8574	-3.5064	-0.6296	-4.7170		3.1678	-0.1386	3.4522	-1.6497
$g \ f_1$	-0.7613	-0.1942	-1.1549	-0.1074	$f'_1$	0.7311	1.2070	0.4008	1.2798
$f \ f_1$	-0.4467	0.1418	-0.8551	0.2319		0.3495	0.8433	0.4008	1.2798
$g \ \varepsilon$	4.1461	3.5609	3.5609	2.9758	$f_0$	-1.6898	-2.5176	-2.5176	-3.3453
$f \ h_1$	-0.2277	0.5968	-0.5030	0.8714	$h'_1$	-0.4221	0.7443	-0.8109	1.1331
$g \ P$	3.5815	3.5815	3.5815	3.5815	$f_2$	0.0000	0.0000	0.0000	0.0000
$f \ O$	4.6362	4.6362	4.6362	4.6362					
$f \ O$	-4.7602	-4.7602	-4.7602	-4.7602					

In the following we will present the model predictions for scattering lengths, bound states, and cross sections.

### A. Effective-range parameters

For ESC08c the  $I = 0$  low-energy parameters are

$$a_{\Lambda\Lambda}(^1S_0) = -0.853 \text{ [fm]}, \quad r_{\Lambda\Lambda}(^1S_0) = 5.126 \text{ [fm]}.$$

$$a_{\Xi N}(^3S_1) = -5.357 \text{ [fm]}, \quad r_{\Xi N}(^3S_1) = 1.434 \text{ [fm]}.$$

For  $I = 1$  we have for ESC08c:

$$a_{\Xi N}(^1S_0) = 0.579 \text{ [fm]}, \quad r_{\Xi N}(^1S_0) = -2.521 \text{ [fm]},$$

$$a_{\Xi N}(^3S_1) = 4.911 \text{ [fm]}, \quad r_{\Xi N}(^3S_1) = 0.527 \text{ [fm]},$$

and for  $I = 2$  we have for ESC08c:

$$a_{\Sigma^\pm\Sigma^\pm}(^1S_0) = +8.10 \text{ } (-0.65) \text{ [fm]},$$

$$r_{\Sigma^\pm\Sigma^\pm}(^1S_0) = -65.36 \text{ } (19.97) \text{ [fm]}.$$

The values in parentheses indicate the values without Coulomb. The results at the  $\Xi N$  threshold and at the  $\Lambda\Sigma$  threshold are given in Table VII-VIII. The  $\Lambda\Lambda(^1S_0)$

given in Table VI.

In Fig. 3 and Fig. 4 we display the OBE potentials for the individual pseudoscalar, vector, scalar, and axial mesons in the case of model ESC08c.

TABLE VII: ESC08c: Inverse-scattering-length and effective-range matrices at (i) the  $\Xi N$  threshold for  $I=0$ , and (ii) the  $\Lambda\Sigma$  threshold for  $I=1$ . The order of the states (1-2) reads  $\Lambda\Lambda(^1S_0)$ ,  $\Xi N(^1S_0)$ , and  $\Xi N(^1S_0)$ ,  $\Lambda\Sigma(^1S_0)$  for respectively  $I=0$  and  $I=1$ . The dimension of the matrix elements are in  $[\text{fm}]^{-1}(A^{-1})$  and  $[\text{fm}](R)$ .

	$\Xi N$ -threshold		$\Lambda\Sigma$ -threshold	
	$A^{-1}$	$R$	$A^{-1}$	$R$
11	0.472	13.001	0.062	11.774
12	1.591	2.088	-1.436	9.744
22	0.870	3.276	-0.736	9.659

scattering lengths are found to be larger in absolute value than in the NSC97 models [7], indicating a more attractive  $\Lambda\Lambda$  interaction.

The old experimental information seemed to indicate a separation energy of  $\Delta B_{\Lambda\Lambda} = 4 - 5$  MeV, corresponding to a rather strong attractive  $\Lambda\Lambda$  interaction. As a matter of fact, an estimate for the  $\Lambda\Lambda(^1S_0)$  scattering length, based on such a value for  $\Delta B_{\Lambda\Lambda}$ , gives  $a_{\Lambda\Lambda}(^1S_0) \approx -2.0$  fm [31, 32]. However, in recent years the experimental information and interpretation of the ground state levels of  $^6_{\Lambda\Lambda}\text{He}$ ,  $^{10}_{\Lambda\Lambda}\text{Be}$ , and  $^{13}_{\Lambda\Lambda}\text{B}$  [33], has been changed drastically. This because of the Nagara-event [8], identified uniquely as  $^6_{\Lambda\Lambda}\text{He}$  [8], which established that the  $\Lambda\Lambda$ -interaction is

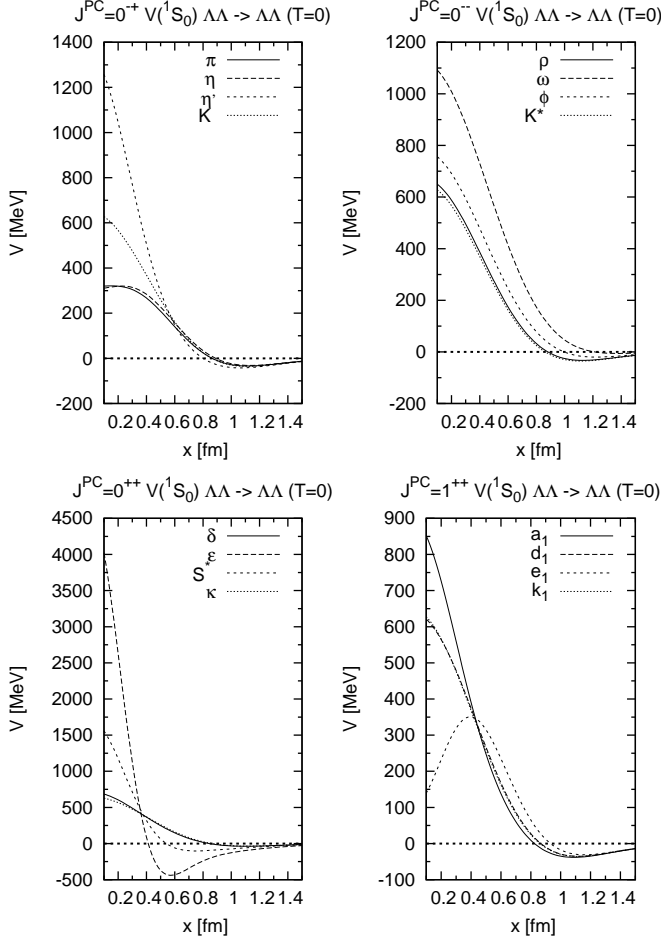


FIG. 3: ESC08c: OBE contributions to the  $\Lambda\Lambda(^1S_0, I = 0)$  potentials for the PS, V, S, and A meson nonets.

TABLE VIII:  $I = 1$ : Inverse-scattering-length and effective-range matrices at the  $\Lambda\Sigma$  threshold. The order of the states (1-2) reads  $\Xi N(^3S_1)$ ,  $\Xi N(^3D_1)$ ,  $\Lambda\Sigma(^3S_1)$ . The dimension of the matrix elements are in  $[\text{fm}]^{-1-l-l'}(A^{-1})$  and  $[\text{fm}]^{1-l-l'}(R)$ .

	ESC08c	
	$A^{-1}$	$R$
11	1.302	1.454
12	-9.122	18.305
13	0.504	1.709
22	239.128	-590.173
23	4.252	-16.637
33	1.030	1.540

weaker ( $\Delta B_{\Lambda\Lambda} \approx 0.7$  MeV).

In NSC97 [14] it was only possible to increase the attraction in the  $\Lambda\Lambda$  channel by modifying the scalar-exchange potential. If the scalar mesons are viewed as being mainly  $q\bar{q}$  states, one finds that the (attractive) scalar-exchange part of the interaction in the various

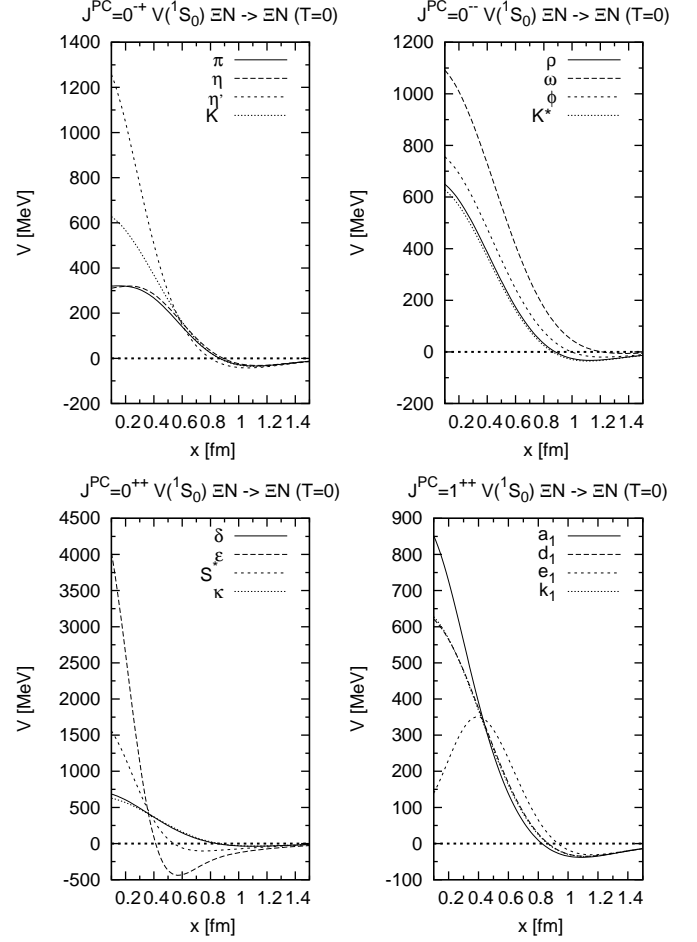


FIG. 4: ESC08c: OBE contributions to the  $\Xi N(^1S_0, I = 0)$  potentials for the PS, V, S, and A meson nonets.

channels satisfies

$$|V_{\Lambda\Lambda}| < |V_{\Lambda N}| < |V_{NN}|, \quad (6.1)$$

suggesting indeed a rather weak  $\Lambda\Lambda$ -potential. The NSC97 fits to the  $YN$  scattering data [14] give values for the scalar-meson mixing angle which seem to point to almost ideal mixing for the scalars as  $q\bar{q}$  states. We found that an increased attraction in the  $\Lambda\Lambda$  channel would give rise to (experimentally unobserved) deeply bound states in the  $\Lambda N$  channel. On the other hand, in the ESC-models there are in principle more possibilities because of the presence of meson-pair potentials. As one sees from the values of the  $a_{\Lambda\Lambda}(^1S_0)$  in the ESC08c model of this paper, we can produce the apparently required attraction in the  $\Lambda\Lambda$  interaction without giving rise to  $\Lambda N$  bound states. Notice that also in ESC08 we have ideal scalar mixings, akin to NSC97.

## B. Deuteron state in $\Xi N(^3S_1 - ^3D_1, I = 1)$

A discussion of the possible bound-states, using the  $SU(3)$  content of the different  $S = 0, -1, -2$  channels is

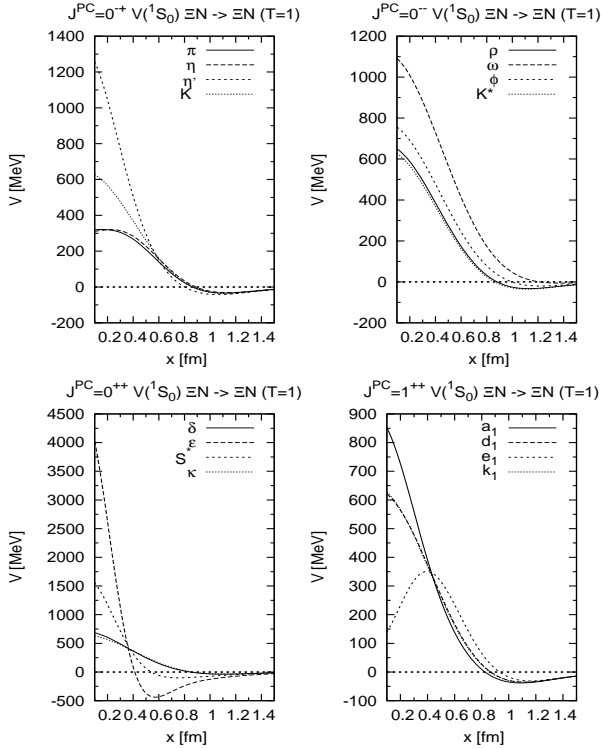
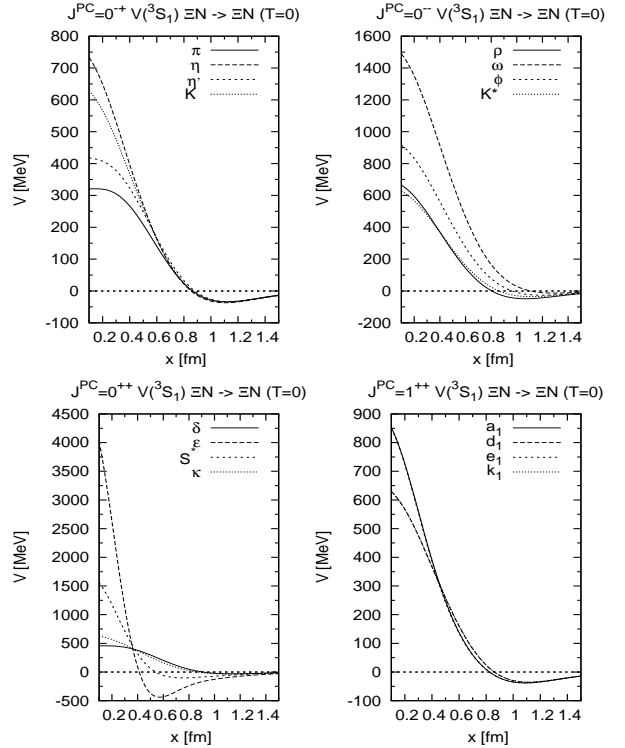
FIG. 5:  $\Xi N(^1S_0, I = 1)$  potentials

TABLE IX: SU(3) content of the different interaction channels.  $S$  is the total strangeness and  $I$  is the isospin. The upper half refers to the space-spin symmetric states  $^3S_1$ ,  $^1P_1$ ,  $^3D$ , ..., while the lower half refers to the space-spin antisymmetric states  $^1S_0$ ,  $^3P$ ,  $^1D_2$ , ...

Space-spin symmetric			
$S$	$I$	Channels	SU(3)-irreps
0	0	$NN$	$\{10^*\}$
-1	1/2	$\Lambda N, \Sigma N$	$\{10^*\}, \{8\}_a$
	3/2	$\Sigma N$	$\{10\}$
-2	0	$\Xi N$	$\{8\}_a$
	1	$\Xi N, \Sigma \Sigma$	$\{10\}, \{10^*\}, \{8\}_a$
		$\Sigma \Lambda$	$\{10\}, \{10^*\}$
Space-spin antisymmetric			
$S$	$I$	Channels	SU(3)-irreps
0	1	$NN$	$\{27\}$
-1	1/2	$\Lambda N, \Sigma N$	$\{27\}, \{8\}_s$
	3/2	$\Sigma N$	$\{27\}$
-2	0	$\Lambda \Lambda, \Xi N, \Sigma \Sigma$	$\{27\}, \{8\}_s, \{1\}$
	1	$\Xi N, \Sigma \Lambda$	$\{27\}, \{8\}_s$
	2	$\Sigma \Sigma$	$\{27\}$

given in [7]. As in [7], for a general orientation, we list in Table IX all the irreps to which the various baryon-baryon channels belong. In ESC08c we find a deuteron with isospin  $I=1$  and strangeness  $S=-2$ , belonging to the  $\{10^*\}$  SU(3)-irrep, which is a  $\Xi N$  bound state in the  $^3S_1$ - $^3D_1$  coupled partial wave. In model ESC04d [5], however, there occurs a  $\Xi N$  bound state in the  $\Xi N(^3S_1$ - $^3D_1r, I = 0)$  partial wave. From Table IX one sees that

FIG. 6:  $\Xi N(^3S_1, I = 0)$  potentials

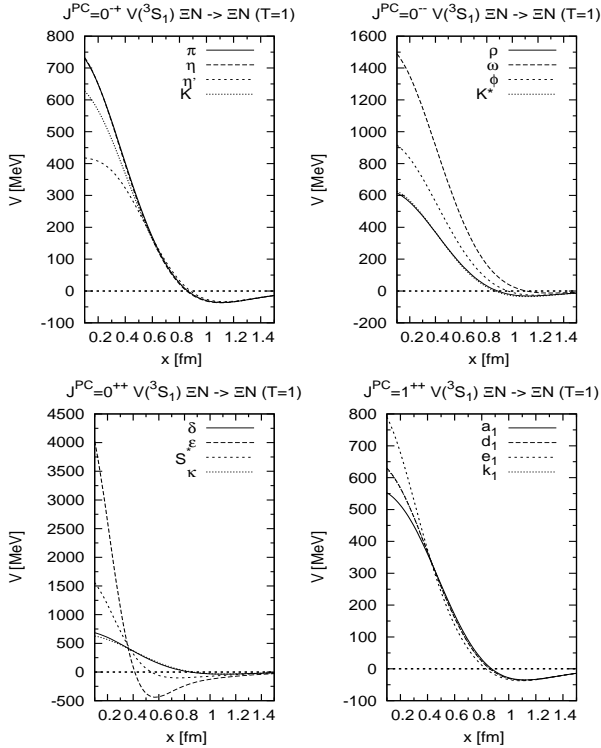
this is a  $\{8_a\}$ -state, which was a little bit surprising, because the OBE-potential one expects to be rather repulsive in the irrep  $\{8_a\}$ , see [15]. In the ESC04 models this occurrence was ascribed to the inclusion of the potentials of the axial-vector-mesons, and the meson pairs. Since ESC04a-c did not show such a bound state it is considered to be accidental. However, the situation in ESC08c is completely different. Here the bound state is in the deuteron-like states where strong tensor forces are present, which causes the binding similarly to the np-deuteron. In Fig. 17 the tensor potentials are shown, where it appears that also the  $\Sigma \Lambda$  tensor potential is important. This is similar to the situation in  $\Lambda N$  below the  $\Sigma N$ -threshold where a large cusp occurs. The calculated binding energy  $B_E(D^*) = 1.56$  MeV.

### C. Partial Wave Phase Parameters

For the  $BB$ -channels below the inelastic threshold we use for the parametrization of the amplitudes the standard nuclear-bar phase shifts [34]. The information on the elastic amplitudes above thresholds is most conveniently given using the BKS-phases [16–18]. For uncoupled partial waves, the elastic  $BB$   $S$ -matrix element is parametrized as

$$S = \eta e^{2i\delta}, \quad \eta = \cos(2\rho). \quad (6.2)$$

For coupled partial waves the elastic  $BB$ -amplitudes are  $2 \times 2$ -matrices. The BKS  $S$ -matrix parametrization,

FIG. 7:  $\Xi N(^3S_1, I = 1)$  potentials

which is of the type-S variety, is given by

$$S = e^{i\delta} e^{i\epsilon} N e^{i\epsilon} e^{i\delta}, \quad (6.3)$$

where

$$\delta = \begin{pmatrix} \delta_\alpha & 0 \\ 0 & \delta_\beta \end{pmatrix}, \quad \epsilon = \begin{pmatrix} 0 & \epsilon \\ \epsilon & 0 \end{pmatrix}, \quad (6.4)$$

and  $N$  is a real, symmetric matrix parametrize as

$$N = \begin{pmatrix} \eta_{11} & \eta_{12} \\ \eta_{12} & \eta_{22} \end{pmatrix}. \quad (6.5)$$

From the various parametrizations of the  $N$ -matrix, we choose the Kabir-Kermode parametrization [19] to represent the  $N$ -matrix in the figures. Then, the  $N$ -matrix is given by the inelasticity parameters  $(\alpha, \beta, \varphi)$ , called  $\rho$ -parameters, as follows

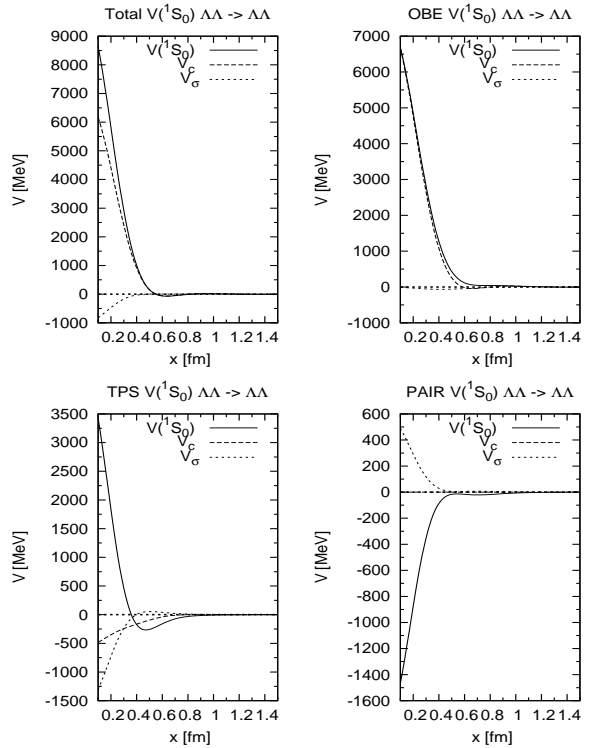
$$N = \begin{pmatrix} \cos(2\alpha) & \sin(\varphi + \xi) \\ \sin(\varphi + \xi) & \cos(2\beta) \end{pmatrix}, \quad (6.6)$$

where

$$\begin{aligned} \alpha &= \pm \frac{1}{2} \cos^{-1}(\eta_{11}), \quad \beta = \pm \frac{1}{2} \cos^{-1}(\eta_{22}), \\ \varphi &= \sin^{-1}(\eta_{12}) - \text{sgn}(\eta_{12}) \sin^{-1} Q \\ \xi &= \text{sgn}(\eta_{12}) \sin^{-1} Q. \end{aligned} \quad (6.7)$$

Here

$$Q^2 = 1 - |\eta_{11} + \eta_{22}| + \eta_{11}\eta_{22}. \quad (6.8)$$

FIG. 8:  $\Lambda\Lambda(^1S_0, I = 0)$  potentials

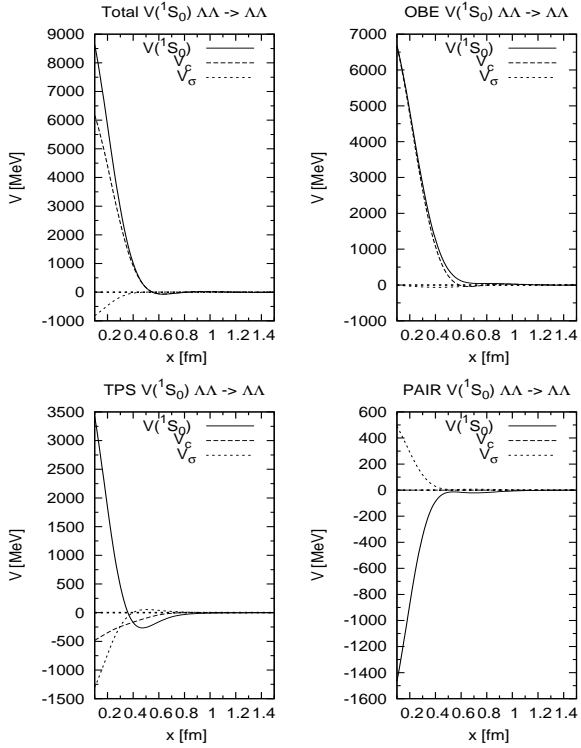
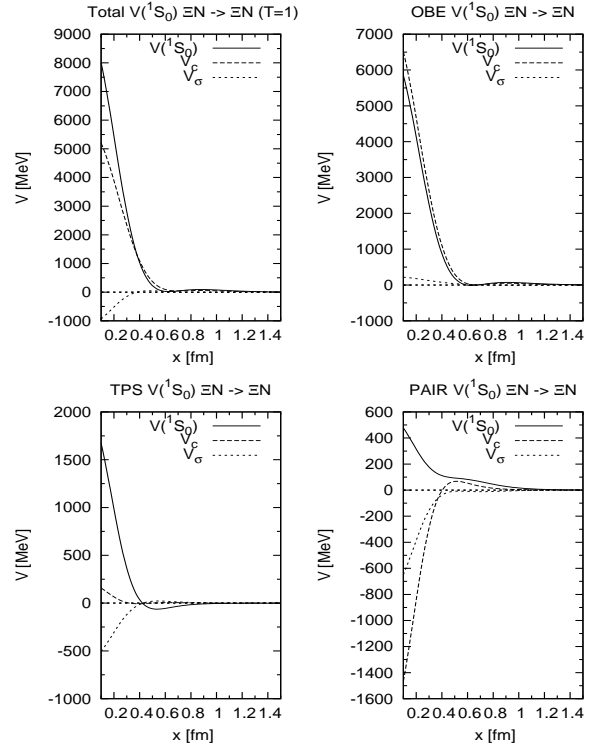
In Fig's 13-16 the BKS-phases and coupling parameters  $(\alpha, \beta, \varphi)$  for ESC08c are shown. In Fig 13 and Fig. 15 we also show the  $^1S_0$ -phases (n.c.) for the case with no coupling to the other two-particle channels. For  $\Lambda\Lambda$  the n.c.-curve shows that the potential is repulsive, which is mainly due to the  $\{1\}$ -irrep. The attraction comes in particular from the coupling to the  $\Xi N$ -channel.

In the Tables XIX-XXV, we give for ESC08c the phases and inelasticity parameters  $\rho$  and  $\eta_{11}, \eta_{12}, \eta_{22}$ , which enable the reader to construct the  $N$ -matrix most directly.

#### D. Total cross sections

We next present the predictions for the total cross section for several channels. We suppose always that the beam as well as the target are unpolarized. Therefore, we incuded the statistical factors, which are  $1/4$  for the spin-singlet and  $3/4$  for the spin-triplet case.

For those cases where both baryons are charged, we do not include the purely Coulomb contribution to the total cross section, nor do we include the Coulomb interference to the nuclear amplitude. The cross section is calculated by summing the contributions from partial waves with orbital angular momentum up to and including  $L = 2$ . We find this to be sufficient for all the  $S \neq 0$  sectors; inclusion of any higher partial waves has no significant effect. Inclusion of higher partial waves will shift the total cross section to slightly higher values without changing

FIG. 9:  $\Xi N(^1S_0, I = 0)$  potentialsFIG. 10:  $\Xi N(^1S_0, I = 1)$  potentials

the overall shape. Of course, their inclusion would be necessary if a detailed comparison with real experimental data were to be made.

In Table X we show the  $\Lambda\Lambda \rightarrow \Lambda\Lambda, \Xi N$  total X-sections as a function of the laboratory momentum  $p_\Lambda$ . Being dominantly S-wave, there is in principle has a (sharp) cusp at the  $\Xi N$ -threshold, i.e.  $p_\Lambda = 344.4 \text{ MeV}/c^2$ , which indeed is visible in the table. In Table X we also show the  $\Xi N \rightarrow \Xi N, \Lambda\Lambda$  total X-sections as a function of the laboratory momentum  $p_\Xi$ . In Table XI we show the total X-sections for the  $\Xi N \rightarrow \Xi N, \Sigma\Lambda$  and the  $I = 1, L = 0$   $\Sigma\Lambda \rightarrow \Sigma\Lambda, \Xi N, \Sigma\Sigma$  reactions as a function of the laboratory momentum  $p_\Xi$ .

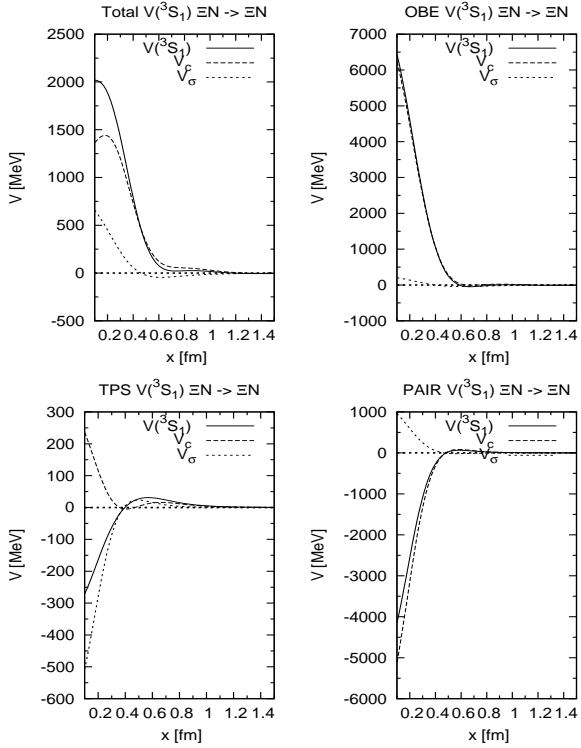
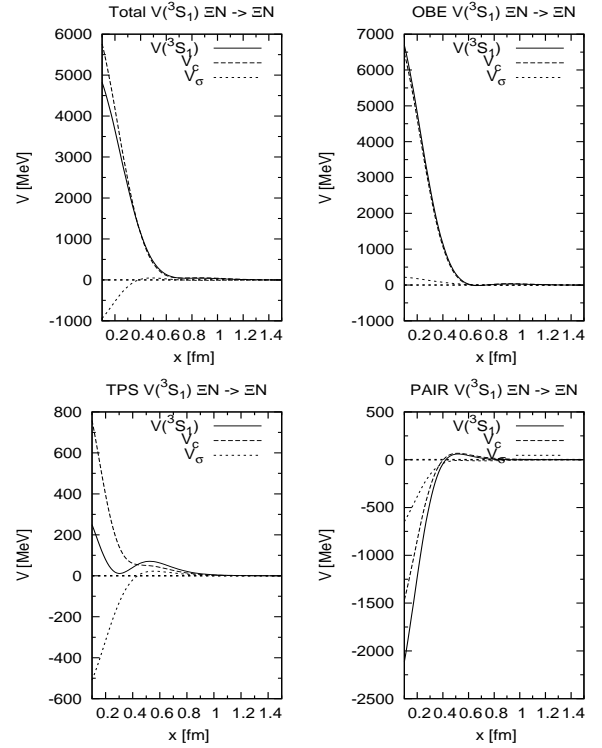
### E. Flavor SU(3)-irrep potentials

In Fig. 20 and 21 the SU(3)-irreps are displayed. The solid lines show averages of the SU(3)-irrep potentials using the potentials on the particle basis. The dashed lines are the irrep potentials in an SU(3) limit, where  $M_N = M_\Lambda = M_\Sigma = M_\Xi = 1115.6 \text{ MeV}$ ,  $m_\pi = m_K = m_\eta = m_{\eta'} = 410 \text{ MeV}$ ,  $m_\rho = m_{K^*} = m_\omega = m_\phi = 880 \text{ MeV}$ , and  $m_{a_0} = m_\kappa = m_\sigma = m_{f_0} = 880 \text{ MeV}$ . Comparison with the results from LQCD [35, 36] shows qualitatively very similar results. The exception is the SU(3)-singlet  $\{1\}$ -irrep. Here LQCD potential is attractive for  $0 < r < \infty$ , whereas in ESC08c there is an attractive pocket for  $r \leq 0.5 \text{ fm}$  and is repulsive for  $r > 0.5 \text{ fm}$ .

TABLE X: ESC08c ( $I = 0, L = 0$ ) total X-sections in [mb] as a function of the laboratory momentum  $p_\Lambda$  in [MeV]

$p_\Lambda$	$\Lambda\Lambda \rightarrow \Lambda\Lambda, \Xi N$		$\Xi N \rightarrow \Xi N, \Lambda\Lambda$	
	$\Lambda\Lambda$	$\Xi N$	$\Xi N$	$\Lambda\Lambda$
10	22.65	—	630.95	2468.24
50	20.98	—	114.35	1817.61
100	16.83	—	49.78	990.75
200	8.58	—	100.01	607.52
300	5.16	—	58.81	405.65
350	6.42	2.28	28.35	161.84
400	6.96	6.68	16.15	85.65
500	11.03	23.39	10.96	55.60
600	6.26	17.50	8.86	41.69
700	4.92	12.78	8.13	33.69
800	4.87	10.40	7.68	29.07
900	5.41	9.05	6.93	27.48
1000	5.69	7.38	6.51	26.94

This shape is due to the behavior of the spin-spin potentials from pseudoscalar and vector exchange, which have zero volume integrals. In the  $\{1\}$ -irrep for the SU(3)-broken potential (solid line) there is no bound state, i.e. no H-particle [37]. This is in agreement with the recent experimental result studying  $\Upsilon(1S, 2S)$ -decay [38].

FIG. 11:  $\Xi N(^3S_1, I = 0)$  potentialsFIG. 12:  $\Xi N(^3S_1, I = 1)$  potentialsTABLE XI: ESC08c ( $I = 1, L = 0$ ) total X-sections  $\Xi N \rightarrow \Xi N, \Sigma \Lambda$  in [mb] as a function of the laboratory momentum  $p_\Xi$  in [MeV]

$p_\Xi$	$\Xi N \rightarrow \Xi N, \Sigma \Lambda$		$\Sigma \Lambda \rightarrow \Sigma \Lambda, \Xi N, \Sigma \Sigma$		
	$\Xi N$	$\Sigma \Lambda$	$\Sigma \Lambda$	$\Xi N$	$\Sigma \Sigma$
10	66.52	—	690.58	10.61	—
50	66.55	—	124.73	8.51	—
100	66.75	—	58.40	6.83	—
200	67.88	—	20.46	10.28	—
300	69.36	—	13.78	17.53	—
400	70.27	—	12.96	21.97	—
500	69.80	—	11.86	36.62	—
600	86.79	2.21	11.70	42.12	—
700	50.02	3.84	10.19	19.67	0.99
800	46.79	5.59	9.84	15.49	1.94
900	42.87	6.58	8.67	26.72	6.32
950	40.71	7.18	7.58	23.74	5.60
1000	45.79	6.37	7.56	49.80	7.83

ESC08c. G-matrix calculations are performed with the continuous (CON) choice, where off-shell potentials are taken into account continuously from on-shell ones in intermediate propagations of correlated pairs. Then, a two-body state is specified by spin  $S$ , isospin  $T$ , orbital and total angular momenta  $L$  and  $J$ , respectively. The imaginary parts of G-matrices appear due to energy-conserving transitions from  $\Xi N$  to  $\Lambda\Lambda$  channels in the  $T = 0$   $^1S_1$  and  $^3P_J$  states. The conversion width  $\Gamma_\Xi^c$  is obtained from the imaginary part of  $U_\Xi$  multiplying by  $-2$ .

TABLE XII:  $U_\Xi(\rho_0)$  and partial wave contributions for ESC08c calculated with the CON choice.  $\Gamma_\Xi^c$  denotes  $\Xi N$ - $\Lambda\Lambda$  conversion width. All entries are in MeV.

$T$	$^1S_0$	$^3S_1$	$^1P_1$	$^3P_0$	$^3P_1$	$^3P_2$	$U_\Xi$	$\Gamma_\Xi^c$
0	1.4	-8.0	-0.3	1.8	1.4	-2.1		
1	10.7	-11.1	1.1	0.7	-2.6	-0.0	-7.0	4.5

## VII. $\Xi N$ G-MATRIX INTERACTION AND $\Xi$ -NUCLEUS STATES<sup>1</sup>

We calculate  $\Xi$  potential energies  $U_\Xi$  and derive  $\Xi N$  G-matrix interactions in nuclear matter with the use of

<sup>1</sup> IN THIS SECTION WE DENOTE ISOSPIN BY T, THE NUCLEAR PHYSICS NOTATION.

Table XII shows the potential energy  $U_\Xi$  and its partial-wave contributions at normal density  $\rho_0$ . The  $U_\Xi$  values turn out to be given by the strong cancellation between attractive contributions in  $^3S_1$  ( $T = 0, 1$ ) states and repulsive contributions in  $^1S_0$  ( $T = 0, 1$ ) states. Eventually, values of  $U_\Xi$  become far less attractive than those of  $U_\Lambda$ . The calculated value of  $\Gamma_\Xi^c(\rho_0)$  is also given in the Table XII, the dominant contribution of which comes from the  $\Lambda\Lambda$ - $\Xi N$ - $\Sigma$  coupling interaction in the

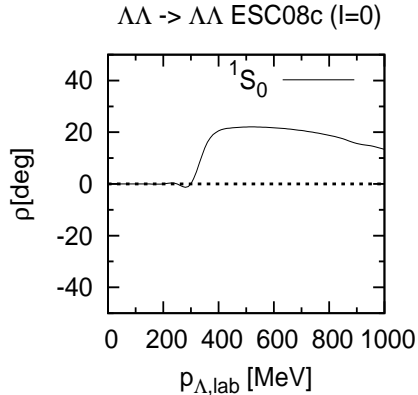
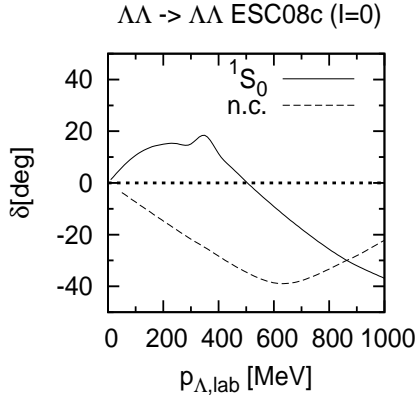


FIG. 13: ESC08c ( $^1S_0, I = 0$ )  $\Lambda\Lambda$ -phases. The dashed curve n.c. is the case with no coupling to the  $\Xi N, \Sigma\Sigma$  channels.

$T = 0$   $^1S_0$  state.

In Fig. 22,  $U_\Xi$  values and partial-wave contributions are drawn as a function of  $k_F$ . Here,  $U_\Xi(k_F)$  is shown by a bold curve, and contributions in  $^{33}S_1$ ,  $^{31}S_1$ ,  $^{13}S_1$  and  $^{31}S_1$  states are shown by thin curves.  $P$ -state contribution summed for  $(S, T, J)$  states is shown by a dashed curve.

As well as in Table XII, we see here the cancellation between attractive contributions in spin-triplet  $S$  states and repulsive ones in spin-singlet  $S$  states. Especially, the attraction in the  $^3S_1$   $T = 1$  state is due to the  $\Xi N$ - $\Lambda\Sigma$ - $\Sigma\Sigma$  tensor-coupling interactions in this state. If these tensor parts in this channel are switched off, the value of  $U_\Xi$  becomes strongly repulsive. On the other hand, the  $P$ -state contributions are small.

It should be noted that the  $U_\Xi$  curve becomes substantially attractive in the low density region due to the strong density dependence. This feature works favorably for  $\Xi$  binding energies in light systems.

For applications to finite  $\Xi$  systems,  $\Xi N$ - $\Xi N$  central parts of the complex G-matrix interactions for ESC08c are represented in Gaussian forms, whose coefficients are given as a function of  $k_F$ . The determined parameters are given in Table XIII.

As demonstrated in Ref. [39], the observed spectra of  $\Lambda$

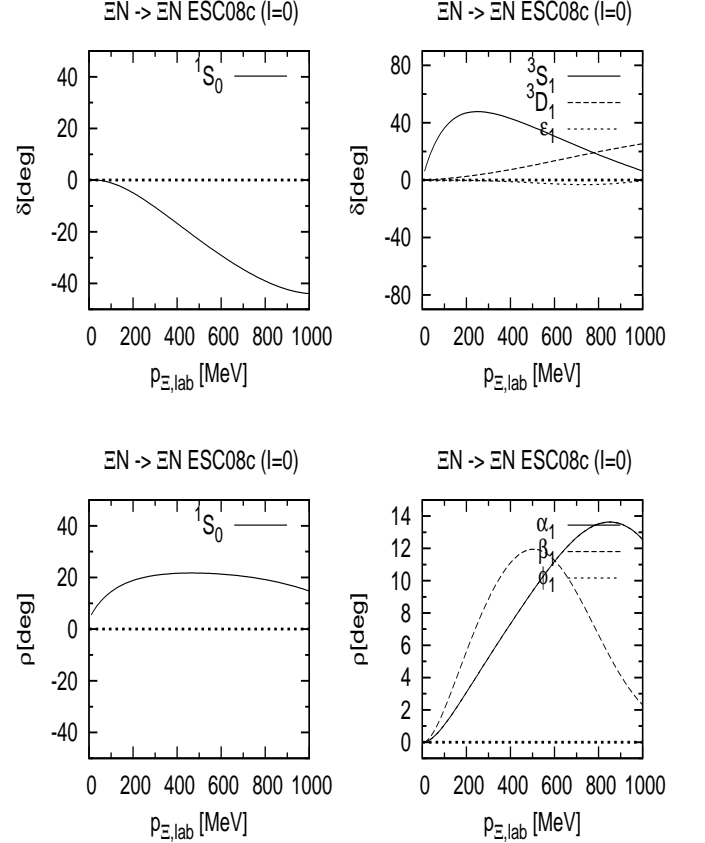


FIG. 14: ESC08c  $I = 0$   $\Xi N$ -phases.

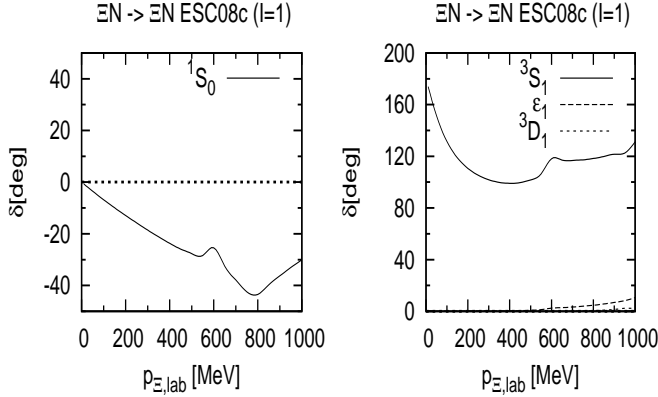
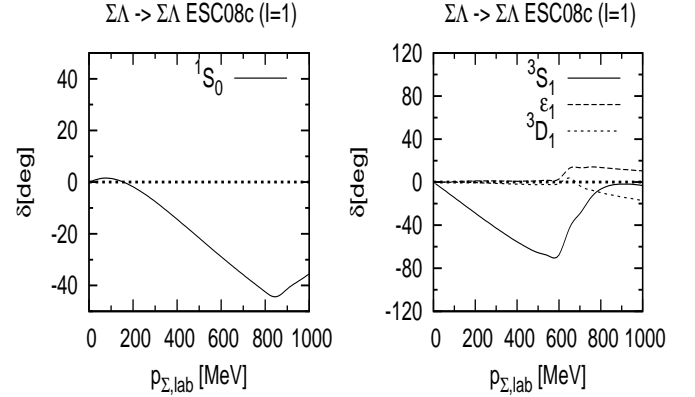
hypernuclei are described successfully with the  $\Lambda$ -nucleus folding potentials derived from the  $\Lambda N$  G-matrix interactions. Here, the same method is applied to  $\Xi^-$ -nucleus systems. A  $\Xi$ -nucleus folding potential in a finite system is obtained from  $\mathcal{G}_{(\pm)}^{TS}(r; k_F)$  as follows:

$$\begin{aligned} U_\Xi(\mathbf{r}, \mathbf{r}') &= U_{dr} + U_{ex}, \\ U_{dr} &= \delta(\mathbf{r} - \mathbf{r}') \int d\mathbf{r}'' \rho(\mathbf{r}'') V_{dr}(|\mathbf{r} - \mathbf{r}''|; k_F) \\ U_{ex} &= \rho(\mathbf{r}, \mathbf{r}') V_{ex}(|\mathbf{r} - \mathbf{r}'|; k_F), \end{aligned} \quad (7.1)$$

$$\begin{pmatrix} V_{dr} \\ V_{ex} \end{pmatrix} = \frac{1}{2(2t_Y + 1)(2s_Y + 1)} \sum_{TS} (2T + 1)(2S + 1) \cdot [\mathcal{G}_{(\pm)}^{TS} \pm \mathcal{G}_{(\mp)}^{TS}], \quad (7.2)$$

where  $(\pm)$  denote parity quantum numbers. Here, core nuclei are assumed to be spherical, and densities  $\rho(r)$  and mixed densities  $\rho(r, r')$  are obtained from Skyrme-HF wave functions. The isospin-dependence of  $\mathcal{G}_{(\pm)}^{TS}(r; k_F)$  leads to the Lane term. In this work, only the diagonal parts of the  $\mathbf{t}_\Xi \cdot \mathbf{T}_c$  term are taken into account.

For  $k_F$  included in  $\mathcal{G}(r; k_F)$ , we use the averaged-density approximation (ADA): An averaged value of  $\rho(r)$  is defined by  $\bar{\rho} = \langle \phi_\Xi(r) | \rho(r) | \phi_\Xi(r) \rangle$  by using a  $\Xi$ -state function  $\phi_\Xi(r)$ . Then, an averaged value of  $k_F$  is given

FIG. 15: ESC08c  $I = 1$   $\Xi N$ -phases.FIG. 16: ESC08c  $I = 1$   $\Sigma\Lambda$ -phases.

by  $\bar{k}_F = (1 + \alpha) (1.5\pi^2 \bar{\rho})^{1/3}$ . This value  $\bar{k}_F$  is put into  $\mathcal{G}(r; k_F)$  and determined self-consistently for each  $\Xi$  state, and  $\alpha$  is a parameter fixed by a fine tuning to the experimental data. Hereafter, we investigate the two cases of  $\alpha = 0.0$  and  $0.1$ .

Table XIV shows the results for  $1S$  and  $2P$  bound states in  $\Xi^- + ^{12}\text{C}$  and  $\Xi^- + ^{14}\text{N}$  systems, where Coulomb interactions between  $\Xi^-$  and  $^{12}\text{C}$  ( $^{14}\text{N}$ ) are taken into account.  $B_{\Xi^-}$  and  $\sqrt{\langle r^2 \rangle}$  are the binding energy and r.m.s. radius of  $\Xi^-$ , respectively. Conversion widths  $\Gamma_{\Xi^-}^c$  come from the imaginary parts included in  $T = 0$   $^1S_0$  and  $^3P$  states. The obtained  $2P$  states become unbound, when the Coulomb interactions between  $\Xi^-$  and  $^{12}\text{C}$  ( $^{14}\text{N}$ ) are switched off. Namely these  $2P$  states are so called Coulomb-assisted bound states. They are specified by the fact that the values of  $\sqrt{\langle r^2 \rangle}$  are large due to their weak binding, but far smaller than those in  $\Xi^-$  atomic states. For instance, we have  $B_{\Xi^-} = 0.175$  MeV and  $\sqrt{\langle r^2 \rangle} = 36$  fm for the  $\Xi^- + ^{14}\text{N}$   $3D$  state.

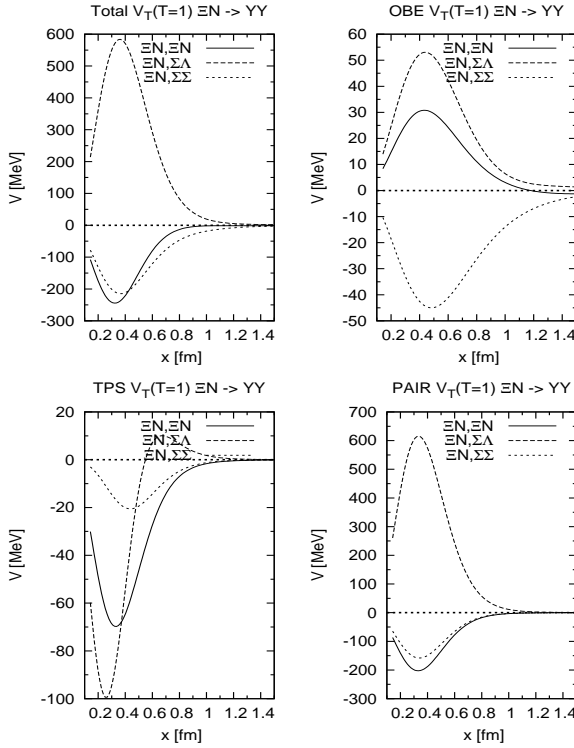
Experimental information for  $\Xi N$  interactions can be obtained from emulsion events of simultaneous emission of two  $\Lambda$  hypernuclei (twin  $\Lambda$  hypernuclei) from a  $\Xi^-$  absorption point. The  $\Xi^-$  produced by the  $(K^-, K^+)$  reaction is absorbed into a nucleus ( $^{12}\text{C}$ ,  $^{14}\text{N}$  or  $^{16}\text{O}$  in emulsion) from some atomic orbit, and by the following  $\Xi^- p \rightarrow \Lambda\Lambda$  process two  $\Lambda$  hypernuclei are produced.

Then, the energy difference between the initial  $\Xi^-$  state and the final twin  $\Lambda$  state gives rise to the binding energy  $B_{\Xi^-}$  between  $\Xi^-$  and the nucleus.

Two events of twin  $\Lambda$  hypernuclei (I) [40] and (II) [41] were observed in the KEK E-176 experiment, and recently the new event (III) [42] has been observed in the KEK E373 experiment. In the cases of (I) and (II), each event has no unique interpretation for its reaction process. However, it is possible to find a consistent understanding for these two events as follows: The events (I) and (II) were interpreted to be reactions of  $\Xi^-$  captured by  $^{12}\text{C}$ . Assuming that the  $\Xi^-$  is absorbed from the  $2P$  orbit in each case, we have consistently the following reactions

$$\begin{aligned} \text{(I)} \quad & \Xi^- + ^{12}\text{C} \rightarrow {}^9_{\Lambda}\text{Be} + {}^4_{\Lambda}\text{H} \quad (B_{\Xi^-} = 0.82 \pm 0.17 \text{ MeV}), \\ \text{(II)} \quad & \Xi^- + ^{12}\text{C} \rightarrow {}^9_{\Lambda}\text{Be}^* + {}^4_{\Lambda}\text{H} \quad (B_{\Xi^-} = 0.82 \pm 0.14 \text{ MeV}). \end{aligned} \quad (7.3)$$

Assuming that the  $\Xi^-$  is captured from a  $2P$  state, the calculated values of  $B_{\Xi^-}(2P)$  in the  $\Xi^- + ^{12}\text{C}$  system (1.10 and 0.68 MeV for  $\alpha = 0.0$  and 0.1, respectively) turn out to be consistent with the values of 0.65  $\sim$  1.00 MeV given by these data. In Ref. [43], this result was used to fit the strength of the  $\Xi N$  interaction. In these two events, however, a possibility cannot be ruled out that they are captured from  $3D$  states.

FIG. 17:  $\Xi N(^3S_1, T = 1)$  tensor potentials

The event (III) is uniquely identified as

$$\Xi^- + {}^{14}\text{N} \rightarrow {}^{10}\Lambda\text{Be} + {}^5\Lambda\text{He}, \quad (7.4)$$

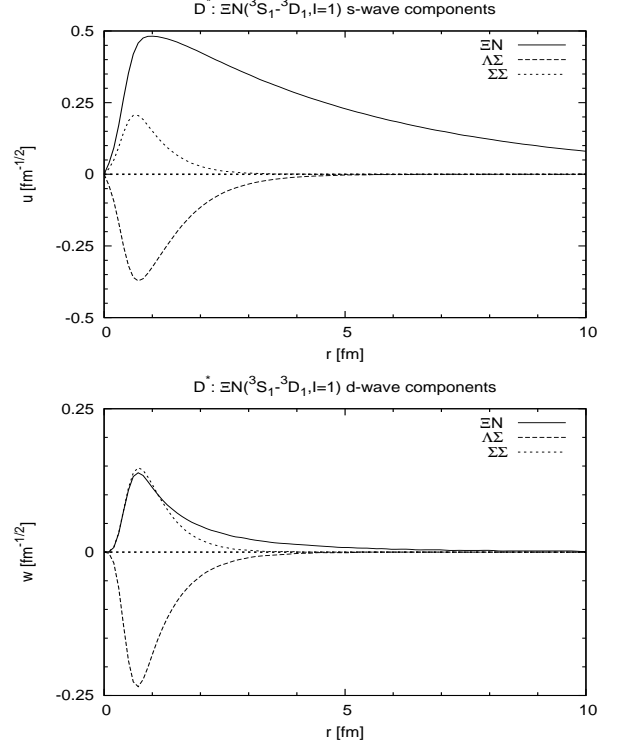
with  $B_{\Xi^-} = 4.38 \pm 0.25$  MeV, which is the first clear evidence of a deeply bound state of the  $\Xi^- - {}^{14}\text{N}$  system. This value can be reproduced by taking  $\alpha = 0.14$ , assuming the  $\Xi^-$  is captured from the  $1S$  state. However, it is far more probable that  ${}^{10}\Lambda\text{Be}$  is produced in some excited state. In Ref. [42], the excitation energies are taken from the theoretical calculations [44] [45], while the ground-state value of  $B_{\Lambda}$  is taken from the emulsion data. Their estimated values of  $B_{\Xi^-}$  are  $1.8 \sim 2.0$  MeV and  $1.1 \sim 1.3$  MeV, when  ${}^{10}\Lambda\text{Be}$  is in the first and second excited state, respectively. Our calculated values of  $B_{\Xi^-}$  ( $2P$ )  $1.85$  and  $1.22$  MeV for  $\alpha = 0.0$  and  $0.1$  are within the former and the latter regions, respectively. The similar value

Hereafter, calculations are performed using the G-matrix interactions with  $\alpha = 0.1$ . Let us demonstrate the results for heavier systems  ${}^{28}\text{Mg}$  and  ${}^{89}\text{Sr}$ , being produced by  $p(K^-, K^+) \Xi^-$  reactions on  ${}^{28}\text{Si}$  and  ${}^{89}\text{Y}$  targets, respectively. In Table XV, we show calculated values of  $\Xi^-$  s.p. energies  $E_{\Xi^-}$ , conversion widths  $\Gamma_{\Xi^-}^c$  and r.m.s radii  $\sqrt{\langle r_{\Xi^-}^2 \rangle}$  of solved  $\Xi^-$  wave functions, where  $\Delta E_L$  and  $\Delta E_C$  are contributions from Lane terms and Coulomb interactions, respectively. It should be noted that the deep  $s$  and  $p$  states are owing to large contribu-

tions from Coulomb attractions.

The BNL-E885 experiment [47] suggests that a  $\Xi^-$  s.p. potential in  ${}^{11}\Xi^-$  Be is given by the attractive Wood-Saxon potential with the depth  $\sim -14$  MeV (called WS14). In this case, the calculated value of  $B_{\Xi^-}$  ( $2P$ ) is  $0.41$  ( $0.79$ ) MeV for the  $\Xi^- + {}^{12}\text{C}$  ( ${}^{14}\text{N}$ ) system, WS14 being slightly less attractive than the above  $\Xi$ -nucleus potentials suitable to the emulsion events of twin  $\Lambda$  hypernuclei,

It is well known that capture probabilities of  $\Xi^-$  from  $2P$  states are far smaller than those from  $3D$  states. In spite of this fact, twin  $\Lambda$  hypernuclei are produced dominantly after  $2P$ - $\Xi^-$  captures. As discussed in Ref. [46],

FIG. 18:  $\Xi N(^3S_1 -> {}^3D_1, I = 1)$  deuteron wave functions

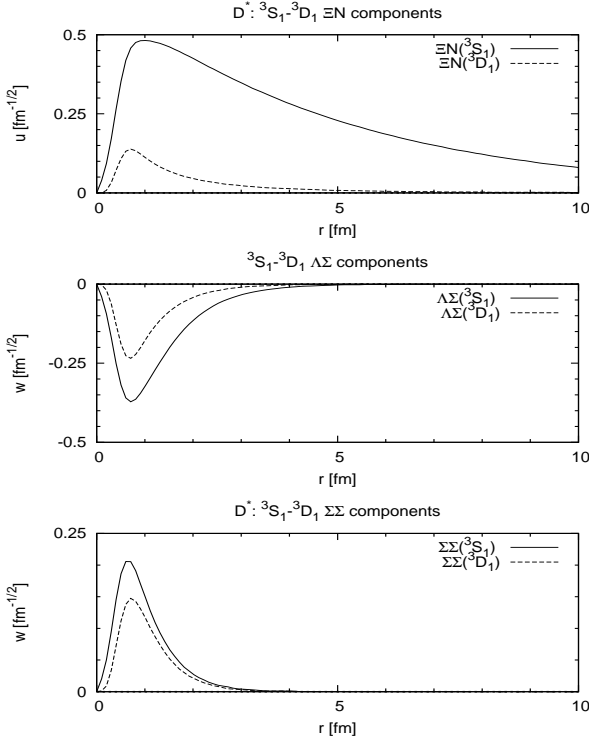
the reason is because sticking probabilities of two  $\Lambda$ 's produced after  $2P$ - $\Xi^-$  captures are substantially larger than those after  $3D$ - $\Xi^-$  captures.

the reason is because sticking probabilities of two  $\Lambda$ 's produced after  $2P$ - $\Xi^-$  captures are substantially larger than those after  $3D$ - $\Xi^-$  captures.

the reason is because sticking probabilities of two  $\Lambda$ 's produced after  $2P$ - $\Xi^-$  captures are substantially larger than those after  $3D$ - $\Xi^-$  captures.

The BNL-E885 experiment [47] suggests that a  $\Xi^-$  s.p. potential in  ${}^{11}\Xi^-$  Be is given by the attractive Wood-Saxon potential with the depth  $\sim -14$  MeV (called WS14). In this case, the calculated value of  $B_{\Xi^-}$  ( $2P$ ) is  $0.41$  ( $0.79$ ) MeV for the  $\Xi^- + {}^{12}\text{C}$  ( ${}^{14}\text{N}$ ) system, WS14 being slightly less attractive than the above  $\Xi$ -nucleus potentials suitable to the emulsion events of twin  $\Lambda$  hypernuclei.

In order to investigate the possibility of observing  $\Xi^-$  hypernuclear state, we calculate  $K^+$  spectra of  $(K^-, K^+)$

FIG. 19:  $\Xi N(^3S_1 - ^3D_1, I = 1)$  deuteron wave functions

reactions on some targets with use of our G-matrix folding potentials. Calculations are performed with the Green's function method in DWIA [48]. In Fig. 23, we show the obtained  $K^+$  spectra for  $^{12}\text{C}$  and  $^{28}\text{Si}$  targets at forward-angle with an incident momentum  $1.65 \text{ GeV}/c$ . We can see clearly the peaks of  $p$ - and  $d$ -bound states, respectively, in the cases of  $^{12}\text{C}$  and  $^{28}\text{Si}$  targets. Here, the experimental resolution is assumed to be 2 MeV. Solid and dotted curves are for ESC08c and WS14, respectively. Strong enhancement of the highest- $L$  state in the ESC08c case is due to the  $k_F$ -dependent effects of G-matrix interactions. When the  $\bar{k}_F$  values for the  $p$  and  $d$  states are taken as the same as those for the  $s$  states, the obtained spectra for ESC08c become similar to those for WS14. We conclude this section by making some remarks on the inclusion of the three-body repulsive (TBR) and attractive (TBA) interactions for  $S=-2$  systems. In the case of the  $\Lambda$ -hypernuclei in paper II [2] an important conclusion from the G-matrix analysis is that the experimental  $B_\Lambda$  values and excited spectra can be reproduced in a natural way by ESC08c. Although the multipomeron (MPP) repulsive contributions are decisively important in the high density region, they should be almost canceled by the three-body attractions (TBA) in the normal density region.

In the case of the  $\Xi$ -hypernuclei it is shown here that the  $\Xi N$  attraction in ESC08c is consistent with the  $\Xi$ -nucleus binding energies given by the emulsion data of the twin  $\Lambda$ -hypernuclei. As in the case of the  $\Lambda$ -

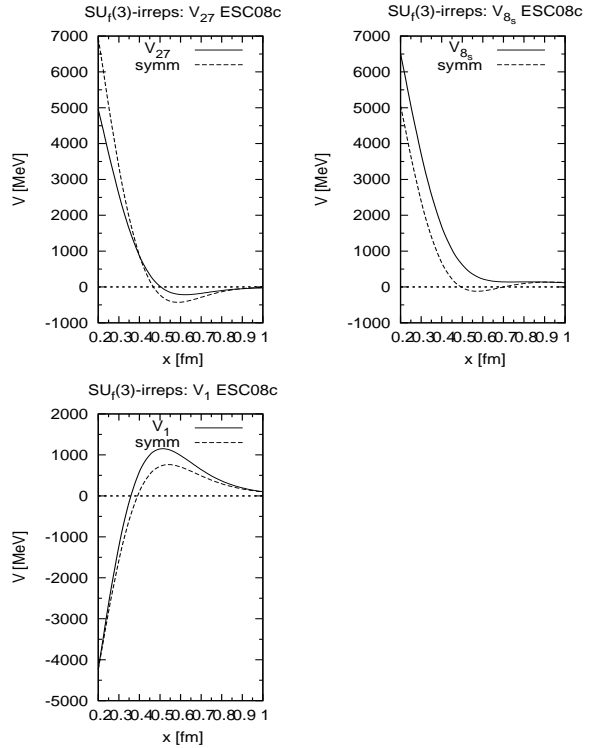


FIG. 20: Solid line average SU(3)-irrep potentials in particle basis. Dashed lines potentials with exact flavor SU(3)-symmetry

hypernuclei, we can expect some role of the MPP+TBA contribution. For a clear analysis, however, the experimental data of  $B_\Xi$  are too scarce. On the other hand, MPP contributions are essential in the problem of  $\Xi$ -mixing in neutron star matter. We defer the discussion and inclusion of the three-body interactions in the  $S=-2$  system, i.e. ESC08c+ model, to a future paper.

## VIII. SUMMARY AND CONCLUSION

The ESC08c model potentials presented here are a major step in constructing the baryon-baryon interactions for scattering and hypernuclei in the context of broken SU(3)-symmetry using, apart from the gaussian repulsion from the Pomeron and inclusion of a systematic quark-core effects for all baryon-baryon channels, generalized yukawian meson-exchange for the dynamics. The potentials are based on (i) One-boson-exchanges, where the coupling constants at the baryon-baryon-meson vertices are restricted by the broken SU(3) symmetry, (ii) Two-pseudoscalar exchanges, (iii) Meson-Pair exchanges. Each type of meson exchange (pseudoscalar, vector, axial-vector, scalar) contains five free parameters: a singlet coupling constant, an octet coupling constant, the  $F/(F+D)$  ratio  $\alpha$ , a meson-mixing angle. The potentials are regularized with gaussian cut-off parameters, which provide a few additional free parameters. As shown in

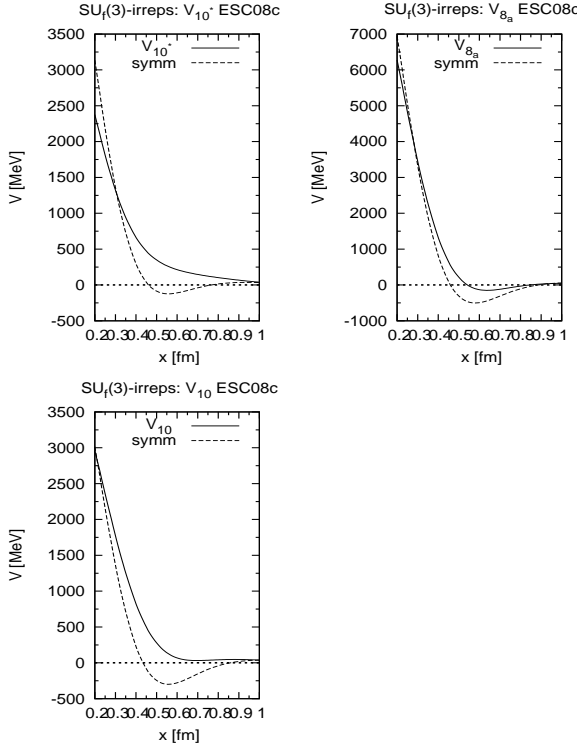


FIG. 21: Solid line average SU(3)-irrep potentials in particle basis. Dashed lines potentials with exact flavor SU(3)-symmetry

paper I and II the  $F/(F + D)$  parameters could be restricted, both for OBE and MPE, by the Quark-model predictions in the form of the  ${}^3P_0$  quark-antiquark creation mechanism.

Although we performed truly simultaneous fits to the  $NN$  and  $YN$  data, effectively most of these parameters are determined in fitting the rich and accurate  $NN$  scattering data, while the remaining ones are fixed by fitting also the (few)  $YN$  scattering data. This still leaves enough flexibility to accomodate the imposition of a few extra constraints. As demonstrated here, the assumption of SU(3) symmetry for the couplings then allows us to extend these models to the higher strangeness channels (i.e.,  $YY$  and all interactions involving cascades), without the need to introduce additional free parameters. Like the NSC97 models, the ESC04 and ESC08 models are very powerful models of this kind, and the very first realistic ones.

The most striking prediction of ESC08c is the existence of the  $S=-2$  deuteron  $D^*$ , below the  $\Xi N$ -threshold. The width is expected to be small since the decay must be isospin breaking and is electromagnetic and/or weak. The experimental search for baryon-baryon bound states by the Rome-Saclay-Vanderbilt collaboration [49] in the mass range 21.-2.5 GeV/c<sup>2</sup> was negative. It could be that the resolution in this experiment was insufficient to detect a very narrow state near the  $\Xi N$ -threshold. It is important to emphasize that the existence of the

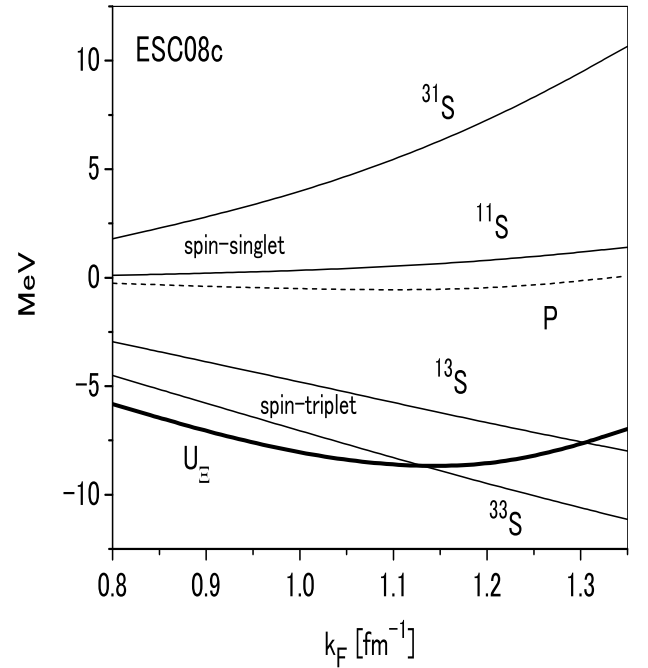


FIG. 22:  $U_{\Xi}$  and partial-wave contributions in  ${}^{(2T+1)(2S+1)}L_J$  states are drawn as a function of  $k_F$ .  $U_{\Xi}(k_F)$  is shown by a bold curve. Attractive contributions in spin-triplet states ( ${}^{33}S_1$  and  ${}^{13}S_1$ ) and repulsive ones in spin-singlet states ( ${}^{31}S_1$  and  ${}^{11}S_1$ ) are shown by thin curves. The  $P$ -state contribution, summed for  $(T, S, J)$ , is shown by a dashed curve.

$D^*$ -state is strongly connected to the  $\Xi$ -nucleus attraction as indicated by experiments, see [47] and the recent emulsion-experiments results [42]. In one of the ESC04-models, ESC04d, the bound  $S=-2$  bound state occurred in the  $\Xi N({}^3S_1, I = 0)$ -channel, which is a member of an SU(3) octet  $\{8_a\}$ -irrep. The ESC08c result is much more natural, fitting nicely with the existence of a  $\{10^*\}$  SU(3)-deuteron multiplet.

In order to illustrate the basic properties of these potentials, we have presented results for scattering lengths, possible bound states in  $S$ -waves, and total cross sections. Although the different versions ESC04 and ESC08 produce the  $NN$  and  $YN$  data well, there are considerable differences. In the NN-sector the quality of the fit to the NN-data of the ESC08-models is superior to that for the ESC04-models. Also, they lead to notable differences in the hypernuclear structures, especially in  $S = -2$  systems. A typical example can be seen in their  $\Xi N$  sectors: The derived  $\Xi$ -nucleus potentials are different from each other even qualitatively. It is quite important that ESC04d and ESC08a,b,c solutions predicts the existence of  $\Xi$ -hypernuclei consistently with the indication given by the BNL-E885 experiment. For a discussion  $\Xi$ -nucleus attraction in the case of the ESC04 and

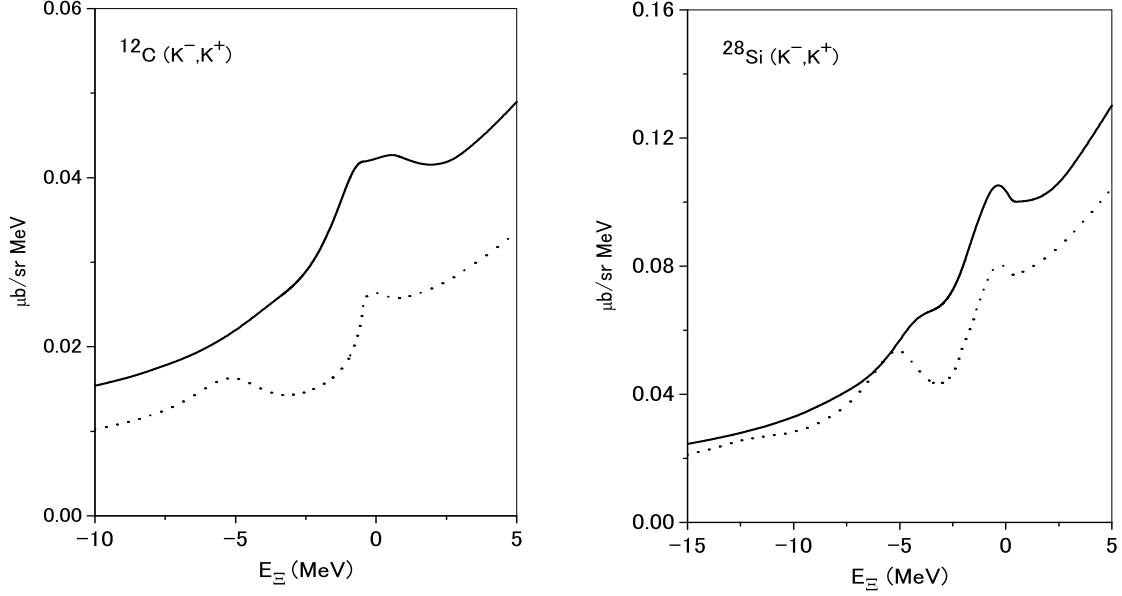


FIG. 23:  $K^+$  spectra of  $(K^-, K^+)$  reactions on  $^{12}\text{C}$  (left panel) and  $^{28}\text{Si}$  (right panel) for ESC08c (solid) and WS14 (dotted).

TABLE XIII:  $\mathcal{G}(r; k_F) = \sum_i (a_i + b_i k_F + c_i k_F^2) \exp(-(r/\beta_i)^2$  in  $^{(2S+1)(2T+1)}E$  and  $^{(2S+1)(2T+1)}O$  states.

	$\beta_i$ (fm)	0.50	0.90	2.00
$^{11}E$	a	-540.0	210.4 - 66.76i	-5.59
	b	4975.	-988.7 + 19.32i	0.0
	c	-2500.	490.4 - 2.675i	0.0
$^{13}E$	a	-4353.	562.8	0.215
	b	6760.	-1065.	0.0
	c	-2456.	408.9	0.0
$^{11}O$	a	0.0	70.88	-5.59
	b	0.0	3.319	0.0
	c	0.0	8.351	0.0
$^{13}O$	a	0.0	15.98 - 77.30i	0.215
	b	0.0	-214.4 + 151.5i	0.0
	c	0.0	185.2 - 95.77i	0.0
$^{31}E$	a	-343.9	111.2	0.357
	b	133.5	-18.08	0.0
	c	-10.00	23.38	0.0
$^{33}E$	a	-809.8	50.29	-1.76
	b	1619.	-213.5	0.0
	c	-633.3	95.44	0.0
$^{31}O$	a	0.0	42.44	0.357
	b	0.0	1.531	0.0
	c	0.0	8.844	0.0
$^{33}O$	a	0.0	-17.26	-1.76
	b	0.0	8.867	0.0
	c	0.0	6.355	0.0

ESC08a,b we refer to [5] and [20] respectively. The  $\Xi$ -nucleus attraction derived from ESC08c is owing to the situation that the  $\Xi N$  interaction in the  $^3S_1$  ( $^{33}S_1$ ) state is substantially attractive. This feature is intimately related to tensor-potential giving a strong Lane term. The

TABLE XIV: Calculated quantities in  $\Xi^- + ^{12}\text{C}$  and  $\Xi^- + ^{14}\text{N}$  systems for  $\alpha=0.0$  and  $0.1$ . Binding energies  $B_{\Xi^-}$  and conversion width  $\Gamma_{\Xi^-}^c$  are in MeV. R.m.s. radius  $\sqrt{\langle r^2 \rangle}$  is in fm.

$\Xi^- + ^{12}\text{C}$	$\alpha = 0.0$	$\alpha = 0.1$
$1S$	$B_{\Xi^-}$	5.18
	$\Gamma_{\Xi^-}^c$	1.77
	$\sqrt{\langle r^2 \rangle}$	2.93
$2P$	$B_{\Xi^-}$	1.10
	$\Gamma_{\Xi^-}^c$	0.75
	$\sqrt{\langle r^2 \rangle}$	5.37
$\Xi^- + ^{14}\text{N}$	$\alpha = 0.0$	$\alpha = 0.1$
$1S$	$B_{\Xi^-}$	6.30
	$\Gamma_{\Xi^-}^c$	2.15
	$\sqrt{\langle r^2 \rangle}$	2.85
$2P$	$B_{\Xi^-}$	1.85
	$\Gamma_{\Xi^-}^c$	1.11
	$\sqrt{\langle r^2 \rangle}$	4.50

mass dependence of  $\Xi$  hypernuclei predicted by ESC08c is rather different from that by the OBE model such as NHC-D. The most striking is that the peculiar  $\Xi N$  hypernuclear states are obtained by ESC08c even in  $s$ - and light  $p$ -shell regions.

We finally mention that these ESC08 potentials also provide an excellent starting point for calculations and predictions of multi-strange systems. The extension of this work to the  $S = -3, 4$ -systems, i.e. comprising all  $\{8\} \otimes \{8\}$  baryon-baryon states, will be the topic of the last paper (IV) in this series.

TABLE XV: Calculated values of  $\Xi^-$  single particle energies  $E_{\Xi^-}$  and conversion widths  $\Gamma_{\Xi^-}^c$  for  $^{28}_{\Xi^-}$ Mg ( $^{27}_{\Xi^-}$ Al+ $\Xi^-$ ) and  $^{89}_{\Xi^-}$ Sr ( $^{88}_{\Xi^-}$ Y+ $\Xi^-$ ).  $\Delta E_L$  and  $\Delta E_C$  are contributions from Lane terms and Coulomb interactions, respectively. Entries are in MeV. R.m.s. radii  $\sqrt{\langle r^2 \rangle}$  are in fm. Coulomb assisted bound states are marked by (\*).

		$E_{\Xi^-}$	$\Delta E_L$	$\Delta E_C$	$\Gamma_{\Xi^-}^c$	$\sqrt{\langle r_{\Xi}^2 \rangle}$
$^{28}_{\Xi^-}$ Mg	<i>s</i>	-7.35	+0.13	-6.65	1.66	3.16
	<i>p</i>	-3.86	+0.08	(*)	0.91	4.32
	<i>d</i>	-0.92	+0.03	(*)	0.24	9.47
$^{89}_{\Xi^-}$ Sr	<i>s</i>	-15.5	+0.63	-13.0	1.85	3.25
	<i>p</i>	-11.9	+0.52	-11.4	1.16	4.23
	<i>d</i>	-8.61	+0.41	(*)	0.74	5.04
	<i>f</i>	-5.37	+0.30	(*)	0.45	5.98

### Acknowledgments

We thank T. Motoba and E. Hiyama for many stimulating discussions.

### Appendix A: Baryon-baryon channels and SU(3)-irreps

In Table XVI and Table XVII we give the relation between the potentials on the isospin basis and the potentials in the SU(3)-irreps.

### Appendix B: Meson-pair coupling constants

In Table XVIII we give the MPE-couplings for model ESC08c.

### Appendix C: BKS-phase parameters

In Tables XIX-XXI we display the BKS-phase parameters for model ESC08c.

TABLE XVI: SU(3)-contents of the various potentials on the isospin basis.

Space-spin antisymmetric states $^1S_0, ^3P, ^1D_2, \dots$		
$\Lambda\Lambda \rightarrow \Lambda\Lambda$	$I = 0$	$V_{\Lambda\Lambda,\Lambda\Lambda} = \frac{1}{40}(27V_{27} + 8V_{8_s} + 5V_1)$
$\Lambda\Lambda \rightarrow \Xi N$	„	$V_{\Lambda\Lambda,\Xi N} = \frac{-1}{40}(18V_{27} - 8V_{8_s} - 10V_1)$
$\Lambda\Lambda \rightarrow \Sigma\Sigma$	„	$V_{\Lambda\Lambda,\Sigma\Sigma} = \frac{\sqrt{3}}{40}(-3V_{27} + 8V_{8_s} - 5V_1)$
$\Xi N \rightarrow \Xi N$	„	$V_{\Xi N,\Xi N} = \frac{1}{40}(12V_{27} + 8V_{8_s} + 20V_1)$
$\Xi N \rightarrow \Sigma\Sigma$	„	$V_{\Xi N,\Sigma\Sigma} = \frac{\sqrt{3}}{40}(2V_{27} + 8V_{8_s} - 10V_1)$
$\Sigma\Sigma \rightarrow \Sigma\Sigma$	„	$V_{\Sigma\Sigma,\Sigma\Sigma} = \frac{1}{40}(V_{27} + 24V_{8_s} + 15V_1)$
$\Xi N \rightarrow \Xi N$	$I = 1$	$V_{\Xi N,\Xi N} = \frac{1}{5}(2V_{27} + 3V_{8_s})$
$\Xi N \rightarrow \Lambda\Sigma$	„	$V_{\Xi N,\Lambda\Sigma} = \frac{\sqrt{6}}{5}(V_{27} - V_{8_s})$
$\Sigma\Lambda \rightarrow \Sigma\Lambda$	„	$V_{\Sigma\Lambda,\Sigma\Lambda} = \frac{1}{5}(3V_{27} + 2V_{8_s})$
$\Sigma\Sigma \rightarrow \Sigma\Sigma$	$I = 2$	$V_{\Sigma\Sigma,\Sigma\Sigma} = V_{27}$

TABLE XVII: SU(3)-contents of the various potentials on the isospin basis.

Space-spin symmetric states $^3S_1, ^1P_1, ^3D, \dots$		
$\Xi N \rightarrow \Xi N$	$I = 1$	$V_{\Xi N,\Xi N} = \frac{1}{3}(V_{10} + V_{10^*} + V_{8_a})$
$\Xi N \rightarrow \Sigma\Lambda$	„	$V_{\Xi N,\Sigma\Lambda} = \frac{\sqrt{6}}{6}(V_{10} - V_{10^*})$
$\Xi N \rightarrow \Sigma\Sigma$	„	$V_{\Xi N,\Sigma\Sigma} = \frac{\sqrt{2}}{6}(V_{10} + V_{10^*} - 2V_{8_a})$
$\Sigma\Lambda \rightarrow \Sigma\Lambda$	„	$V_{\Sigma\Lambda,\Sigma\Lambda} = \frac{1}{2}(V_{10} + V_{10^*})$
$\Sigma\Lambda \rightarrow \Sigma\Sigma$	„	$V_{\Sigma\Lambda,\Sigma\Sigma} = \frac{\sqrt{3}}{6}(V_{10} - V_{10^*})$
$\Sigma\Sigma \rightarrow \Sigma\Sigma$	„	$V_{\Sigma\Sigma,\Sigma\Sigma} = \frac{1}{6}(V_{10} + V_{10^*} + 4V_{8_a})$
$\Xi N \rightarrow \Xi N$	$I = 0$	$V_{\Xi N,\Xi N} = V_{8_a}$

TABLE XVIII: Pair coupling constants for model ESC08c, divided by  $\sqrt{4\pi}$ .  $I(M)$  refers to the isospin of the pair  $M$  with quantum-numbers  $J^{PC}$ .

Pair	$J^{PC}$	Type	$I(M)$	$NNM$	$\Sigma\Sigma M$	$\Sigma\Lambda M$	$\Xi\Xi M$	$I(M)$	$\Lambda N M$	$\Lambda\Xi M$	$\Sigma N M$	$\Sigma\Xi M$
$\pi\eta$	$0^{++}$	$g$	1	-1.2371	-2.4742	0.0000	-1.2371	1/2	2.1427	-2.1427	1.2371	1.2371
			0	-2.1427	0.0000	0.0000	2.1427					
$\pi\pi$	$1^{--}$	$g$	1	0.2703	0.5406	0.0000	0.2703	1/2	-0.4682	0.4682	-0.2703	-0.2703
			0	0.4682	0.0000	0.0000	-0.4682					
$\pi\pi$	$1^{--}$	$f$	1	-1.6592	-1.3274	-1.1495	0.3318	1/2	1.7243	-0.5748	-0.3318	1.6592
			0	-0.5748	1.1495	-1.1495	1.7243					
$\pi\rho$	$1^{++}$	$g$	1	5.1287	4.1030	3.5533	-1.0257	1/2	-5.3299	1.7766	1.0257	-5.1287
			0	1.7766	-3.5533	3.5533	-5.3299					
$\pi\sigma$	$1^{++}$	$g$	1	-0.2988	-0.2391	-0.2070	0.0598	1/2	0.3106	-0.1035	-0.0598	0.2988
			0	-0.1035	0.2070	-0.2070	0.3106					
$\pi\omega$	$1^{+-}$	$g$	1	-0.2059	-0.1648	-0.1427	0.0412	1/2	0.2140	-0.0713	-0.0412	0.2059
			0	-0.0713	0.1427	-0.1427	0.2140					

TABLE XIX: ESC08c  $^1S_0(\Lambda\Lambda \rightarrow \Lambda\Lambda)$  BKS-phase parameters in [degrees] as a function of the laboratory momentum  $p_\Lambda$  in [MeV]

$p_\Lambda$	$\delta(^1S_0)$	$\rho(^1S_0)$	$\delta(^3P_0)$	$\rho(^3P_0)$	$\delta(^3P_1)$	$\rho(^3P_1)$	$\delta(^3P_2)$	$\epsilon_2$	$\delta(^3F_2)$
10	1.23	—	-0.00	—	0.00	—	0.00	0.00	0.00
50	5.94	—	-0.00	—	0.01	—	0.02	0.00	0.00
100	10.67	—	-0.04	—	0.10	—	0.18	0.00	0.00
200	14.96	—	-0.35	—	0.57	—	1.30	0.02	0.00
300	15.06	—	-1.17	—	1.19	—	3.95	0.13	0.03
350	18.43	13.90	-1.66	0.71	1.40	0.29	6.39	0.30	0.07
400	11.31	20.52	-2.12	4.48	1.48	1.80	10.78	0.72	0.16
500	5.63	22.04	-3.56	9.92	1.07	4.59	14.55	2.81	0.36
600	-9.11	21.73	-5.07	14.51	-0.12	7.22	-5.00	3.61	0.58
700	-17.82	20.65	-5.92	19.01	-1.84	9.51	-8.75	4.04	0.83
800	-25.64	18.80	-5.56	23.66	-3.67	11.53	-10.75	4.76	1.11
900	-32.03	15.64	-3.43	28.44	-4.47	13.85	-12.81	5.81	1.65
1000	-36.88	13.35	0.02	33.25	-7.46	21.89	-14.18	6.75	1.03

TABLE XX: ESC08c  $^1S_0, ^1P_1(\Xi N \rightarrow \Xi N, I=0)$  BKS-phase parameters in [degrees] as a function of the laboratory momentum  $p_\Xi$  in [MeV]

$p_\Xi$	$\delta(^1S_0)$	$\rho(^1S_0)$	$\delta(^1P_1)$	$\rho(^1P_1)$
10	0.08	5.45	0.00	0.00
50	0.25	11.85	0.05	0.00
100	-0.30	15.88	0.33	0.00
200	-4.17	19.78	1.23	0.00
300	-10.09	21.40	1.50	0.00
350	-13.37	21.79	1.22	0.00
400	-16.72	22.00	0.64	0.00
500	-23.34	22.00	-1.31	0.00
600	-29.54	21.56	-4.11	0.00
700	-35.03	20.72	-7.50	0.00
800	-39.55	19.44	-11.23	0.00
900	-42.78	17.51	-15.13	0.00
1000	-43.87	14.78	-19.11	0.00

TABLE XXI: ESC08c  $^1S_0(\Xi N \rightarrow \Xi N, I = 1)$  etc. BKS-phase parameters in [degrees] as a function of the laboratory momentum  $p_\Xi$  in [MeV]

$p_\Lambda$	$\delta(^1S_0)$	$\rho(^1S_0)$	$\delta(^3P_0)$	$\rho(^3P_0)$	$\delta(^3P_1)$	$\rho(^3P_1)$	$\delta(^3P_2)$	$\epsilon_2$	$\delta(^3F_2)$
10	-0.70	—	-0.00	—	0.00	—	0.00	0.00	-0.00
50	-3.46	—	-0.04	—	0.04	—	0.00	0.00	-0.00
100	-6.75	—	-0.29	—	0.30	—	0.02	0.01	-0.00
200	-12.79	—	-1.32	—	1.55	—	0.08	0.12	-0.01
300	-18.35	—	-2.39	—	3.18	—	0.03	0.35	-0.05
350	-20.95	—	-2.80	—	3.92	—	-0.12	0.48	-0.07
400	-23.37	—	-3.12	—	4.52	—	-0.39	0.62	-0.10
500	-27.15	—	-3.45	—	5.24	—	-1.33	0.76	-0.12
600	-24.30	17.88	-3.31	0.61	5.55	1.35	-2.82	1.12	-0.13
700	-37.01	24.33	-2.37	5.39	5.49	7.50	-4.74	1.31	-0.05
800	-44.30	25.12	-0.89	11.40	4.39	11.77	-6.93	1.46	0.10
900	-37.14	25.06	0.28	18.12	2.47	14.93	-9.26	1.60	0.31
1000	-31.01	24.57	-0.21	24.24	-0.00	17.31	-11.65	1.73	0.58

TABLE XXII: ESC08c  $^1S_0, ^3S_1 - ^3D_1(\Xi N \rightarrow \Xi N, I = 0)$  BKS-phase parameters in [degrees] as a function of the laboratory momentum  $p_\Xi$  in [MeV]

$p_\Xi$	$\delta(^1S_0)$	$\rho(^1S_0)$	$\delta(^3S_1)$	$\epsilon_1$	$\delta(^3D_1)$	$\eta_{11}$	$\eta_{12}$	$\eta_{22}$
10	0.08	5.45	6.19	0.00	0.00	1.00	0.00	1.00
50	0.25	11.85	27.52	0.20	0.00	1.00	0.00	1.00
100	-0.30	15.88	42.78	0.87	-0.00	1.00	0.03	1.00
200	-4.17	19.78	51.04	2.47	-0.08	0.99	0.11	0.99
300	-10.09	21.40	49.00	4.48	-0.32	0.98	0.18	0.98
400	-16.72	22.00	43.88	7.06	-0.87	0.97	0.24	0.97
500	-23.34	22.00	37.52	10.12	-1.77	0.95	0.28	0.95
600	-29.54	21.56	30.65	13.41	-2.81	0.92	0.29	0.92
700	-35.03	20.72	23.85	16.71	-3.47	0.90	0.27	0.90
800	-39.55	19.44	17.52	19.87	-3.32	0.89	0.23	0.89
900	-42.78	17.51	11.74	22.77	-2.24	0.89	0.18	0.89
1000	-43.87	14.78	6.42	25.31	-0.37	0.91	0.14	0.91

TABLE XXIII: ESC08c  $^1S_0, ^3S_1 - ^3D_1(\Xi N \rightarrow \Xi N, I = 1)$  BKS-phase parameters in [degrees] as a function of the laboratory momentum  $p_\Xi$  in [MeV]

$p_\Xi$	$\delta(^1S_0)$	$\rho(^1S_0)$	$\delta(^3S_1)$	$\epsilon_1$	$\delta(^3D_1)$	$\eta_{11}$	$\eta_{12}$	$\eta_{22}$
10	-0.70	0.00	173.90	0.00	-0.00	1.00	-0.00	1.00
50	-3.48	0.00	151.56	0.03	-0.00	1.00	-0.00	1.00
100	-6.80	0.00	131.47	0.11	-0.01	1.00	-0.00	1.00
200	-12.91	0.00	110.65	0.23	-0.10	1.00	-0.02	1.00
300	-18.55	0.00	101.81	0.28	-0.27	1.00	-0.05	1.00
400	-23.69	0.00	99.08	0.36	-0.43	1.00	-0.08	1.00
500	-27.67	0.00	101.75	0.75	-0.44	0.99	-0.13	0.99
600	-25.39	17.43	118.13	2.44	-0.26	0.77	-0.14	0.99
700	-37.88	23.74	116.81	3.32	0.06	0.45	-0.16	0.98
800	-43.46	24.45	118.30	4.69	0.57	0.33	-0.20	0.97
900	-36.27	24.31	121.57	6.81	1.45	0.28	-0.23	0.95
1000	-30.08	23.74	131.27	10.53	2.15	0.34	-0.26	0.93

TABLE XXIV: ESC08c  $^1S_0, ^3S_1 - ^3D_1$  ( $\Sigma\Lambda \rightarrow \Sigma\Lambda, I = 1$ ) BKS-phase parameters in [degrees] as a function of the laboratory momentum  $p_\Xi$  in [MeV]

$p_\Sigma$	$\delta(^1S_0)$	$\rho(^1S_0)$	$\delta(^3S_1)$	$\epsilon_1$	$\delta(^3D_1)$	$\eta_{11}$	$\eta_{12}$	$\eta_{22}$
10	0.32	6.17	-1.42	0.00	-0.00	1.00	-0.00	1.00
50	1.34	13.32	-7.13	0.07	-0.00	0.88	-0.00	1.00
100	1.43	17.66	-14.35	0.40	-0.04	0.77	-0.00	1.00
200	-1.80	21.80	-28.78	1.09	-0.44	0.60	-0.02	1.00
300	-7.51	23.57	-42.69	1.11	-1.16	0.48	-0.03	1.00
400	-14.37	24.31	-55.47	0.85	-1.90	0.39	-0.03	1.00
500	-21.64	24.46	-65.61	1.20	-2.31	0.33	-0.07	0.99
600	-28.87	24.18	-67.63	2.90	-1.25	0.31	-0.17	0.97
700	-35.84	23.54	-29.29	13.38	-3.45	0.19	-0.16	0.83
800	-42.45	22.62	-6.47	13.61	-9.76	0.19	-0.08	0.87
900	-41.35	21.45	-1.81	11.92	-13.71	0.28	-0.07	0.88
1000	-35.53	20.11	-3.05	10.41	-17.07	0.36	-0.09	0.89

TABLE XXV: ESC08c  $I = 2, L = 0, L = 1$   $\Sigma^\pm \Sigma^\pm \rightarrow \Sigma^\pm \Sigma^\pm$  BKS-phase parameters in [degrees] as a function of the laboratory momentum  $p_\Xi$  in [MeV]. In parentheses the phases without Coulomb are listed.

$p_\Sigma$	$\delta(^1S_0)$	$\delta(^3P_0)$	$\delta(^3P_1)$	$\delta(^3P_2)$	$\epsilon_2$	$\delta(^3F_2)$
10	-12.35 (0.94)	-0.20 ( 0.00)	-0.22 ( -0.00)	-0.21 ( 0.00)	0.00	-0.00 ( 0.00)
50	-13.72 (4.26)	-3.08 ( 0.19)	-3.41 ( -0.12)	-3.27 ( 0.01)	0.00	-0.01 ( 0.00)
100	-5.59 (6.46)	-6.41 ( 1.17)	-8.24 ( -0.71)	-7.44 ( 0.11)	0.04	-0.59 ( 0.00)
200	-3.03 (4.75)	-1.01 ( 4.46)	-8.24 ( -2.82)	-4.66 ( 0.79)	0.43	-3.25 ( 0.05)
300	-7.40 (-1.50)	1.54 ( 5.86)	-9.17 ( -4.88)	-2.44 ( 1.86)	1.07	-2.68 ( 0.22)
400	-14.47 (-9.65)	0.36 ( 3.95)	-10.07 ( -6.49)	-0.85 ( 2.73)	1.63	-2.05 ( 0.48)
500	-22.56 (-18.44)	-3.51 (-0.41)	-10.63 ( -7.53)	0.08 ( 3.18)	1.94	-1.49 ( 0.76)
600	-30.91 (-27.29)	-8.89 (-6.14)	-10.59 ( -7.84)	0.57 ( 3.31)	1.91	-1.10 ( 0.93)
700	-39.15 (-35.91)	-14.98(-12.50)	-9.76 ( -7.29)	0.82 ( 3.30)	1.56	-1.03 ( 0.84)
800	-42.88 (-44.18)	-21.31(-19.04)	-8.14 ( -5.88)	0.90 ( 3.17)	0.94	-1.36 ( 0.36)
900	-35.25 (-37.94)	-27.63(-25.53)	-5.96 ( -3.86)	0.75 ( 2.85)	0.15	-2.15 (-0.54)
1000	-28.00 (-30.50)	-33.80(-31.84)	-3.57 ( -1.62)	0.30 ( 2.25)	0.71	-3.37 (-1.87)

- 
- [1] M.M. Nagels, Th.A. Rijken, and Y. Yamamoto, *Extended-soft-core Baryon-Baryon Model ESC08c, I. Nucleon-Nucleon Scattering*, [arXiv:nucl-th/1408.4825].
- [2] M.M. Nagels, Th.A. Rijken, and Y. Yamamoto, *Extended-soft-core Baryon-Baryon Model ESC08c, II. Hyperon-Nucleon Interactions*, [arXiv:nucl-th/1501.06636].
- [3] Th.A. Rijken, *Extended-soft-core Baryon-Baryon Model. I, Nucleon-Nucleon Interactions*, Phys. Rev. **C73**, 044007 (2006) [arXiv:nucl-th/0603041]
- [4] Th.A. Rijken and Y. Yamamoto, *Extended-soft-core Baryon-Baryon Model. II, Hyperon-Nucleon Interactions*, Phys. Rev. **C73**, 044008 (2006) [arXiv:nucl-th/0603042]
- [5] Th.A. Rijken and Y. Yamamoto, *Extended-soft-core baryon-baryon model III, hyperon-hyperon/nucleon interactions*, arXiv:nucl-th/060807 (2006)
- [6] Th.A. Rijken, M.M. Nagels, and Y. Yamamoto, Progr. Theor. Phys. Suppl. **185** (2010) 14.
- [7] V.G.J. Stoks and Th.A. Rijken, Phys. Rev. C **59**, 3009 (1999).
- [8] H. Takahashi, et al., Phys. Rev. Lett. **87**, 212502 (2001).
- [9] M. Danysz, et al., Nucl. Phys. **49** 121 (1963).
- [10] D. J. Prowse, Phys. Rev. Lett. **17** 782 (1966).
- [11] L. Micu, Nucl. Phys. **B10**, 521 (1969); A. Le Yaouanc, L. Oliver, O. P'ene, and j.C. Raynal, Phys. Rev. **D8**, 2223 (1973); **9**, 1415 (1974).
- [12] Th.A. Rijken, *Baryon-baryon Couplings in the  $^3P_0$  and  $^3S_1$  QPC-models*, Notes University of Nijmegen, The Netherlands, *nn-online*, THEF 12.01.
- [13] N. Isgur and J. Paton, Phys. Rev. **D31**, 2910 (1985); R. Kokoski and N. Isgur, Phys. Rev. **D35**, 907 (1987); T.J. Burns and F.E. Close, Phys. Rev. **D74**, 034003 (2006).
- [14] Th.A. Rijken, V.G.J. Stoks, and Y. Yamamoto, Phys. Rev. C **59**, 21 (1999).
- [15] P.M.M. Maessen, Th.A. Rijken, and J.J. de Swart, Phys. Rev. C **40**, 2226 (1989).
- [16] R.A. Bryan, Phys. Rev. C **24**, 2659 (1981); **30** 305 (1984).
- [17] S. Klarsfeld, Phys. Lett. **126b**, 148 (1983).
- [18] D.W.L. Sprung, Phys. Rev. C **32**, 699 (1985).
- [19] A. Kabir and M.W. Kermode, J.Phys.G:Nucl.Phys. **13** (1987) 501.
- [20] Y. Yamamoto, T. Motoba, and Th.A. Rijken, Progr. Theor. Phys. Suppl. **185** (2010) 72.
- [21] M.M. Nagels, T.A. Rijken, and J.J. de Swart, Ann. Phys. (N.Y.) **79**, 338 (1973).
- [22] P.M.M. Maessen, private communication.
- [23] J.J. de Swart, Rev. Mod. Phys. **35**, 916 (1963); **37**, 326(E) (1965).
- [24] E.U. Condon and G.H. Shortley, *The Theory of Atomic Spectra* (Cambridge University Press, Cambridge, England, 1935).
- [25] R.H. Thompson, Phys. Rev. D **1**, 110 (1970).
- [26] Th.A. Rijken, Ann. Phys. (N.Y.) **208**, 253 (1991).
- [27] Th.A. Rijken and V.G.J. Stoks, Phys. Rev. C **46**, 73 (1992); **46**, 102 (1992).
- [28] Th.A. Rijken and V.G.J. Stoks, Phys. Rev. C **54**, 2851 (1996); **54**, 2869 (1996).
- [29] J.J. de Swart, M.M. Nagels, T.A. Rijken, and P.A. Verhoeven, Springer Tracts Mod. Phys. **60**, 138 (1971).
- [30] J.J. de Swart and C.K. Iddings, Phys. Rev. **128**, 2810 (1962); *ibid* **130**, 319 (1963).
- [31] Y.C. Tang and B.C. Herndon, Phys. Rev. **138**, B637 (1965).
- [32] A.R. Bodmer and S. Ali, Phys. Rev. **138**, B644 (1965).
- [33] R.H. Dalitz, D.H. Davis, P.H. Fowler, A. Montwill, J. Pniewski, and J.A. Zakrewski, Proc. Roy. Soc. (London) **A426**, 1 (1989).
- [34] H.P. Stapp, T. Ypsilantis, and N. Metropolis, Phys. Rev. **105**, 302 (1957).
- [35] T. Inoue et al, Phys. Rev. Lett. **106** (2011) 162002.
- [36] T. Inoue et al, Nucl. Phys. **A 881** (2012) 28.
- [37] R.L. Jaffe, Phys. Rev. Lett. **38** (1977) 195; **38** (1977) 617.
- [38] B.H. Kim et al, *search for an H-dibaryon with mass near  $2m_A$  in  $\Upsilon(1S, 2S)$  decays*, arXiv:1302.4028v1 [hep-ex] 17 Feb. 2013.
- [39] Y. Yamamoto, T. Motoba, Th.A. Rijken, Prog. Theor. Phys. Suppl. **No.185** (2010), 72.
- [40] S. Aoki et al., Prog. Theor. Phys. **89** (1993), 493.
- [41] S. Aoki et al., Phys. Lett. **B355** (1995), 45.
- [42] K. Nakazawa et al., Prog. Theor. Exp. Phys. **2015**, 033D02.
- [43] M. Yamaguchi, K. Tominaga, Y. Yamamoto, and T. Ueda, Prog. Theor. Phys. **105** (2001), 627.
- [44] E. Hiyama and Y. Yamamoto, Prog. Theor. Phys. **128** (2012), 105.
- [45] D.J. Millener, Nucl. Phys. A **881** (2012), 298.
- [46] Y. Yamamoto, T. Motoba, T. Fukuda, M. Takahashi, and K. Ikeda, Prog. Theor. Phys. Suppl. **No.117** (1994), 281.
- [47] T. Fukuda et al., Phys. Rev. **C58** (1998), 1306. P. Khaustov et al., Phys. Rev. **C61** (2000), 054603.
- [48] Tadokoro,S., Kobayashi,H., Akaishi,Y.:  $\Xi^-$ -hypernuclear states in heavy nuclei. Phys. Rev. **C51**, 2656-2663 (1995)
- [49] D'Agostini et al, *Rome-Saclay-Vanderbilt collaboration*, Nucl. Phys. **B209**, 1 (1982).